2014-05-07

Analysis of Extracellular ATP Distribution in the Intervertebral Disc Using a Finite Element Model

Byron C. Hsu
University of Miami, bcf.hsu@gmail.com

UNIVERSITY OF MIAMI

ANALYSIS OF EXTRACELLULAR ATP DISTRIBUTION IN THE INTERVERTEBRAL DISC USING A FINITE ELEMENT MODEL

By

Byron Che-Fu Hsu

A THESIS

Submitted to the Faculty
of the University of Miami
in partial fulfillment of the requirements for
the degree of Master of Science

Coral Gables, Florida

May 2014

UNIVERSITY OF MIAMI

A thesis submitted in partial fulfillment of
the requirements for the degree of
Master of Science

ANALYSIS OF EXTRACELLULAR ATP DISTRIBUTION IN THE INTERVERTEBRAL DISC USING A FINITE ELEMENT MODEL

Byron Che-Fu Hsu

Approved:

_____ Chun-Yuh Charles Huang, Ph.D. Assistant Professor of Biomedical Engineering	_____ Alicia Jackson, Ph.D. Assistant Professor of Biomedical Engineering
_____ Francesco Travascio, Ph.D. Assistant Professor of Industrial Engineering	_____ M. Brian Blake, Ph.D. Dean of the Graduate School

HSU, BYRON CHE-FU (M.S., Biomedical Engineering)
Analysis of Extracellular ATP Distribution in the Intervertebral Disc Using a Finite Element Model. (May 2014)

Abstract of a thesis at the University of Miami.

Thesis supervised by Professor Chun-Yuh Charles Huang.
No. of pages in text. (57)

Extracellular adenosine triphosphate (ATP) released from cells can mediate a diverse number of biological responses, such as cell secretion, inflammation, and immune reactions through signaling pathways. According to Wang et al. (2013), the extracellular ATP concentration has been measured to accumulate to a high level in the nucleus pulposus (NP) region in the intervertebral disc (IVD), approximately 165 μM. Since extracellular ATP is involved in a variety of cellular activities, the role of ATP distribution and accumulation in the IVD should be investigated. The objective of this study is to examine the effects of mechanical compression on the distribution of extracellular ATP and its adenine derivatives in the IVD using triphasic mechano-electrochemical theory. This theory describes the mechanical behavior and transport phenomena of charged hydrated soft tissue such as the IVD. Michaelis-Menten kinetics was used to model ATP hydrolysis and incorporated into a finite element model.

Experiments were performed to measure Michaelis-Menten parameters of annulus fibrosus (AF) and NP cells. Results of the ATP hydrolysis experiments show that the maximum reaction velocity, $V_{max,}$ for AF cells is significantly greater than the value for NP cells. Thus, the extracellular ATP hydrolysis rate for AF cells could be significantly greater than the rate for NP cells. By comparing the results with the findings reported by

Wang et al. (2013), the theoretical analysis indicated that mechanical loading may promote ATP hydrolysis and induce an intrinsic cellular response. Based on a finite element model, this study simulates the distribution of extracellular ATP and its adenine derivatives in the IVD under mechanical loading.

ACKNOWLEDGMENTS

I would like to thank Dr. Huang for his mentorship during my time spent working in his lab. You have provided invaluable wisdom and insight into becoming a skilled researcher. I am honored to have participated in your research group. I appreciate the feedback that Dr. Travascio and Dr. Jackson gave me to improve this thesis.

I would also like to thank Daniela for teaching me useful laboratory skills and providing advice about the research process. I appreciate the expertise that Xin and Qiaoqiao provided me when I was troubleshooting. In addition, Yu-Fu and Amaris have been truly supportive in guiding me in the lab.

I would like to thank my parents for making graduate school possible. You have made many sacrifices to help me achieve this milestone.

TABLE OF CONTENTS

Page

LIST OF FIGURES

LIST OF TABLES

Chapter 1—Introduction

Lower back pain is a major economic burden in the United States, with a lifetime prevalence estimated to be 80-90% of the population. It may be associated with disc degeneration of the intervertebral disc (IVD), which occurs due to mechanical factors and a loss of nutrient supply. Understanding the cause of disc degeneration could eventually lead to a treatment for alleviating lower back pain.

1.1 Structure and Function of the IVD

The IVD is an inhomogeneous and anisotropic soft tissue that lies between adjacent vertebrae in the spine. Because it is the largest avascular tissue in the human body, diffusion is the primary mode of nutrient transport. The main function of the IVD is to transfer loads and permit proper spinal movement (1).

Three distinct anatomical regions exist: nucleus pulposus (NP), annulus fibrosus (AF), and cartilaginous endplate (CEP) (Figure 1-1). NP tissue is located in the central portion of the disc, and it is composed of chondrocytic cells, collagen fibrils, and proteoglycans. Negatively charged proteoglycans attract water molecules, producing a swelling pressure found in the center of the IVD. As a result, the water content in NP tissue is higher than AF tissue. Moreover, the NP region contains collagen fibers with random orientation.

AF tissue composition is significantly different from NP tissue (Figure 1-2). AF tissue is made of 15-25 distinct layers of collagen fiber lamellae organized into concentric rings around the NP (2). This structure allows it to resist tensile forces during spinal movement. In addition, it contains mostly type I collagen with a relatively low

proteoglycan and water content. Differences in metabolism also exist between AF and NP cells. For example, NP has a lower collagen content than AF but higher proteoglycan content. The CEP is a thin layer of hyaline cartilage (1 mm thick) and forms an interface between the disc vertebral body (3).

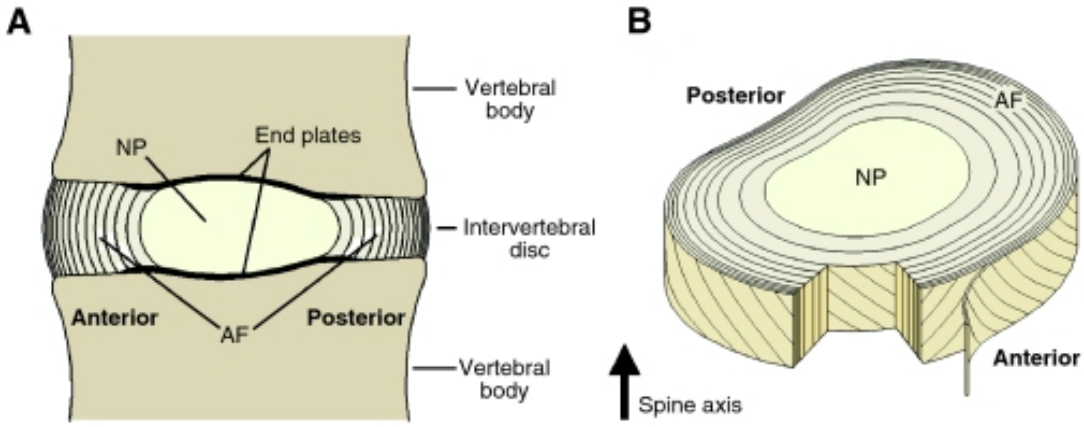

Figure 1-1: Structure of the IVD. The nucleus pulposus (NP), annulus fibrosus (AF), and cartilaginous endplate (CEP) are three main regions of the IVD. (A) The mid-sagittal view and (B) three-dimensional cross section are shown (4).

Due to the avascular nature of the IVD, nutrients such as glucose are supplied to the disc's cells almost entirely by diffusion. Since nutrients must be transported through the tissue, concentration gradients can develop and are dependent upon the supply of nutrients, the rate of nutrient transport through the IVD extracellular matrix (ECM), and the rate of cellular metabolism by disc cells (5). Convective transport, caused by load-induced fluid movement in and out of the disc, is another mechanism of transport for some nutrients (6). However, convection may not be a significant factor for small solutes (7). Blood vessels on the edge of the IVD provide nutrition to the outer AF, while the NP receives nutrients that diffuse through the endplate from the blood supply of the vertebrae (8). As a person

ages, the endplate calcifies and facilitates development of disc degeneration by restricting nutrient transport.

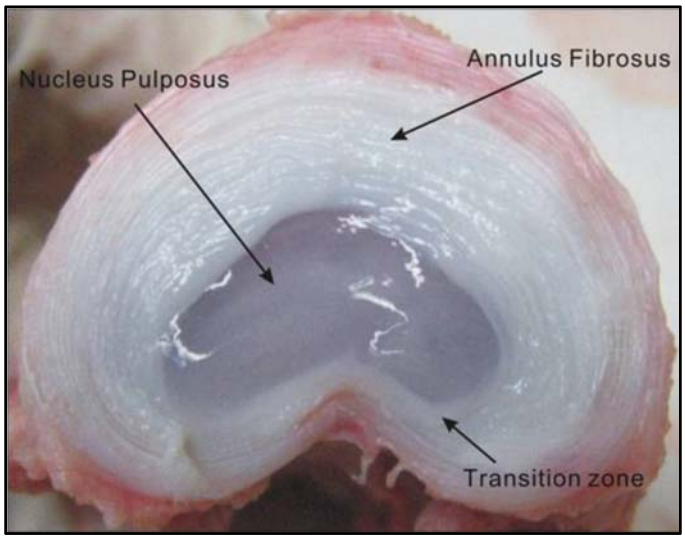

Figure 1-2: Image of IVD. Transverse plane view of porcine intervertebral disc.

A previous study by Wang et al. (2013) reported a high accumulation of extracellular adenosine triphosphate (ATP) in the NP region of the IVD (165 μM) (9). It is a significant finding that needs to be further investigated because extracellular ATP accumulating in avascular tissue may have an important effect on IVD cell function.

1.2 Function of ATP and Adenine Derivatives

The ATP molecule is a nucleoside triphosphate that is involved in intracellular energy transfer (Figure 1-3). Because ATP is present in nearly every cell of the body, it is an important molecule that is involved in the energetics of nearly all cellular activities. For example, IVD cells consume glucose and oxygen in order to produce intracellular ATP and provide energy for extracellular matrix (ECM) synthesis. In contrast, extracellular ATP released from cells can mediate a diverse number of biological responses, such as cell secretion, inflammation, and immune reactions through signaling pathways (10).

Extracellular ATP is known to regulate cell metabolism and growth through purinergic signal pathways, via P2 receptors (11). These receptors are categorized into two main types: G-protein coupled or ligand-gated. After binding purinergic receptors, extracellular ATP may act as a mediator to activate the purinergic pathway. ATP can be hydrolyzed into adenosine diphosphate (ADP), which modulates cellular responses (i.e. proliferation, growth) via purinergic P2Y receptors (12, 13).

In vivo, ATP exists as a neutral molecule because negative charges on the phosphate groups of ATP are electrostatically stabilized by a magnesium (Mg^{2+}) ion. Moreover, ATP must be bound to a magnesium ion to be biologically active and be hydrolyzed at a significant rate (14) (15).

NTPDase1, a member of the ENTPDase family of eight ecto-enzymes, is known to hydrolyze extracellular nucleoside tri- and/or diphosphates such as ATP directly to adenosine monophosphate (AMP) (16). NTPDase2 has a high preference for ATP, while the hydrolysis of ATP by NTPDase3 and NTPDase8 may result in a transient accumulation of ADP (17). Extracellular ATP is hydrolyzed by ectonucleotidases such as NTPDase1, and releases inorganic pyrophosphates (PP_i) and phosphates (P_i). Thus, pyrophosphates and phosphates may lead to calcium deposition in the IVD. Chondrocytes are known to express a specific ectoenzyme, nucleotide triphosphate pyrophosphohydrolase (NTPPPH) that directly degrades ATP to AMP and inorganic pyrophosphate (18). ATP hydrolysis releases chemical energy by breaking phosphoanhydride bonds to generate ADP and orthophosphate (P_i). The overall reaction results in more stable molecules by lowering the Gibbs free energy. ADP can be further hydrolyzed to form AMP and P_i, while AMP can be degraded into adenosine and P_i. ATP is reported to break down rapidly into adenosine in

the bloodstream by ectonucleotidases, and it may contain antinociceptive properties (19). In contrast to ATP, adenosine is known to act on P1 receptors and has anti-inflammatory properties (20). The accumulation of these adenine derivatives will be evaluated in this study to understand their distribution in the IVD.

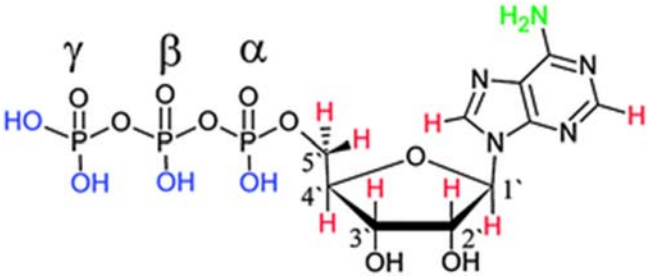

Figure 1-3: Structure of adenosine triphosphate (ATP) molecule (21). ATP contains three phosphate groups and an adenine attached to a ribose sugar.

.

Recently, Wang et al. (2013) found a high accumulation of extracellular ATP in the NP region and was measured to be approximately 165 μM. Due to the biological effects of extracellular ATP and its adenine derivatives, their distribution could exert a significant influence on IVD function and needs to be further investigated.

1.3 Michaelis-Menten Kinetics

The Michaelis-Menten equation has been applied to ATP hydrolysis in previous studies for various processes (22, 23). In this study, ATP hydrolysis is modeled by Michaelis-Menten kinetics and incorporated into a theoretical model. The Michaelis-Menten model illustrates the kinetic properties of enzymes, which enhance the rate of reaction. The Michaelis-Menten equation is:

$$V = \frac{V_{\max}[S]}{[S] + K_M} \qquad (1\text{-}1)$$

where V is the reaction velocity, V_{max} is the maximal velocity, [S] is the concentration of substrate, and K_M is the Michaelis constant. V varies with the substrate concentration [S] in a hyperbolic curve until it reaches V_{max} asymptotically (Figure 1-4). V_{max} is the number of substrate molecules converted into product by an enzyme in a unit time when the enzyme is fully saturated with substrate. The kinetic parameters V_{max} and K_M can be graphically depicted below:

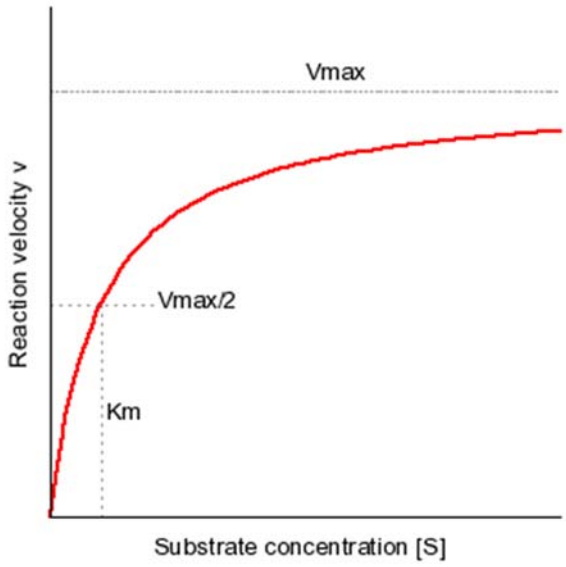

Figure 1-4: Michaelis-Menten plot. A plot of the reaction velocity (V) as a function of the substrate concentration [S] for an enzyme that obeys Michaelis-Menten kinetics shows that the maximal velocity (V_{max}) is approached asymptotically.

K_M is the Michaelis constant, which is equal to the substrate concentration at which the reaction rate is half its maximal value. For most enzymes, the value of K_M is typically between 10^{-1} and 10^{-7} M. K_M is a measure of the strength of the enzyme-substrate (ES) complex: a high K_M indicates weak binding, while a low K_M indicates strong binding.

In a previous study, Huang et al. (2007) used the Michaelis-Menten equation to describe the association between oxygen consumption rate and concentration by IVD cells.

The rates differed significantly between NP and AF cells because glycolysis was the main pathway for ATP production in NP cells. V_{max} and K_M values between these two cell types may vary significantly for ATP hydrolysis.

1.4 Mechanobiological Pathway

Because the primary function of the IVD is to support physical loads, significant mechanical loading is exerted on the IVD. Mechanical loading can be generated at high magnitudes within the disc by fluid flow, hydrostatic pressure, deformation, or tension. Static compression at moderate levels (0.4 MPa) increased proteoglycan and collagen synthesis in explant cultures, while dynamic compression at low frequencies (0.01 Hz, 1 MPa) applied to rodent IVD increased anabolic gene expression of type I and II collagen in NP cells (24-26). IVD cells also differ in response to mechanical stimuli according to cell origin, loading type, magnitude and duration (27). Cells of the innermost NP and AF respond to low-to-moderate magnitudes of static compression, osmotic pressure, or hydrostatic pressure with increases in anabolic cell responses. Large hydrostatic pressures, but little volume change, may occur for NP cells in response to compressive loading. On the other hand, AF cells experience minimal tensile strains in response to tensile loading (27).

A previous study investigated the effects of mechanical loading on IVD cells embedded in an agarose cylindrical construct in a bioreactor (28). Static and dynamic compressive loading on the cell-agarose construct increased total ATP content in AF cells, while NP cells increased total ATP content only during dynamic loading. The same study showed that mechanical loading affects IVD energy metabolism and depends on cell type and loading. A recent study also showed that mechanical loading altered extracellular ATP

accumulation in the IVD, indicating that mechanical compression may regulate extracellular ATP metabolism (9). Because previous studies have shown that extracellular ATP mediates ECM production of chondrocytes under mechanical loading, this effect may also apply to the IVD (29, 30). Therefore, an understanding of how mechanical loading affects extracellular ATP distribution and metabolism in the IVD may be important.

1.5 Triphasic Mechano-Electrochemical Theory

Due to the difficulty of investigating the transport of solutes and mechanical events in the IVD *in vivo*, theoretical modeling has served as a useful tool for examining solute transport and biomechanical behavior of the IVD. Several mathematical models have been developed to describe biomechanical behavior of soft tissues (31, 32). Snijders et al. (1992) developed a triphasic mixture model that did not consider chemical expansion stress (33). Another similar formulation was developed by Huyghe in 1997, who created a quadriphasic mixture model that included electrical fluxes and potential gradients (34).

Among the theoretical frameworks that have been proposed to model soft tissues, one of them is biphasic theory that was formulated by Mow et al. (1980) to describe porous media as a continuum and consisting of an elastic solid matrix embedded in a fluid phase (35). Triphasic theory is an extension of biphasic theory by integrating ion concentration and electrical potential (36).

In 1991, Lai et al. formulated the triphasic mechano-electrochemical theory for porous media, describing the mechanical behavior and transport phenomena of charged hydrated soft tissues (36). Proteoglycans are modeled as a negative charge density fixed to the solid matrix, and monovalent ions in the interstitial fluid are modeled as additional fluid phases. The triphasic mechano-electrochemical theory, based on a tertiary-mixture theory

and the laws of thermodynamics, has been successfully used to study the swelling, negative osmosis and osmotic pressure, transport of fluid and ions, and electrokinetic phenomena in charged hydrated tissues (37).

Gu et al. (1998) extended the triphasic model by proposing a more general mixture theory to account for the presence of multiple electrolytes in tissues (38). It was developed into a comprehensive theory by describing mechanical properties, swelling, and passive transport of multi-electrolytes in the IVD (39-41). Next, Yao et al. (2003) created a theoretical model based on triphasic theory to study dynamic compression within cartilage. They applied triphasic theory to show that chemical, mechanical, and electrical signals may contribute to the response of cartilage to mechanical loading (42).

Recently, the triphasic mixture theory incorporating cellular metabolic rates was able to describe the distribution of nutrients and metabolites in the IVD under the influences of mechanical loads and endplate calcification (43). The triphasic model has been used to analyze exogenous administration of IGF-1 (a potential treatment for disc degeneration) in the IVD via intradiscal injection (44). The mechano-electrochemical mixture model could also be used to examine the transport of extracellular ATP and its adenine derivatives in the IVD under the influence of mechanical loading.

The mechano-electrochemical mixture model considers soft charged tissues such as the IVD as multiphasic. They consist of proteins such as proteoglycans, interstitial water, soluble electrolytes such as NaCl, and cell residing in the interstitial space (45). The IVD can be modeled using a triphasic finite element formulation of mechano-electrochemical theory. Since the theoretical model for investigating mechano-electrochemical behavior of soft hydrated tissue is complex, obtaining an analytical solution for boundary-value

problems is challenging. Thus, the finite element method is a useful numerical tool for handling complicated geometry and boundary conditions. A finite element formulation for triphasic theory has been developed by Sun et al. (1999) (45).

The triphasic mechano-electrochemical theory is based on continuum mechanics and the second law of thermodynamics. It considers a charged hydrated soft tissue as a mixture consisting of: (a) an intrinsically incompressible, porous-permeable-charged solid phase, (b) an intrinsically incompressible interstitial fluid phase, and (c) ion phase with monovalent ion species, anion (-) and cation (+) (45). This mixture is affected by the electrochemical potential of the phases. According to triphasic theory, the gradients of the electrochemical potential drive mechanical deformation of the tissue and fluid flow. The foundation of the current finite element model is multiphasic mechano-electrochemical theory because it presents a comprehensive set of equations to describe biomechanical behavior of the IVD and considers many phases (i.e. water, solid, fluid) in porous media.

Chapter 2—Significance of Study

2.1 Significance

As stated before, lower back pain is associated with disc degeneration. Cells consume nutrients in the IVD and use intracellular ATP as an energy source, while energy production may be a limiting factor for ECM synthesis in maintaining disc integrity. Thus, reduced nutrient supply may be a potential mechanism for disc degeneration (4, 9). However, the relationship between disc degeneration and extracellular ATP has not yet been elucidated.

Recently, a previous study reported a high accumulation of extracellular ATP in the NP region of the IVD (9). Since ATP and its adenine derivatives can mediate a variety of cellular activities, the investigation of their distribution in the IVD could lead to significant findings. Therefore, the objective of this study is to analyze the distribution of extracellular ATP and its adenine derivatives in the IVD using the triphasic mechano-electrochemical model.

2.2 Specific Aims

In this study, a Michaelis-Menten kinetics model was used to account for the hydrolysis rates of ATP and its derivatives. In addition, the Michaelis-Menten parameters for NP and AF cells were determined from ATP hydrolysis experiments. The effects of mechanical compression on the distribution of extracellular ATP and its derivatives were also examined.

Specific Aim 1: to develop a numerical tool that accounts for the consumption and production rates of extracellular ATP and its adenine derivatives. This tool is

useful because the accumulation of adenine derivatives in the IVD are difficult to measure *in vivo*, so a theoretical model can provide a prediction for concentration values. This study aims to contribute knowledge about these neutral solutes in order to further understand their function in the IVD.

Specific Aim 2: to predict the effect of mechanical loading on ATP hydrolysis in the theoretical model. Previous experiments have shown that both static and dynamic compression significantly reduced extracellular ATP content in the NP region (9). The finite element model was implemented to correspond to the general range of measurements made by Wang et al. (2013). A simulation of mechanical compression was used to predict changes in the concentration of extracellular ATP and its adenine derivatives, which could affect\t the rate of ATP hydrolysis.

Chapter 3—Materials and Methods

3.1.1 Triphasic Mechano-Electrochemical Theory

In this study, the IVD was modeled using triphasic mechano-electrochemical theory. In the model, the IVD consists of a solid phase (i.e. collagen and proteoglycan), fluid phase (i.e. water), sodium (Na^+), chloride (Cl^-), and neutral solutes (i.e. ATP, ADP, AMP). Several multiphasic continuity equations are summarized below. First, conservation of mass requires each component the following:

$$\frac{\partial \rho}{\partial t} + \text{div}(\rho \mathbf{v}) = 0 \tag{3-1}$$

where ρ is the mass density, and v is the velocity of component.

For negatively-charged tissue such as the IVD, Na^+ and Cl^- ion concentrations in tissue are related to the absolute value of the negative fixed charged density (c^F) through the electroneutrality condition:

$$c^+ = c^- + c^F \tag{3-2}$$

The net electrical charge is zero because both the FCD and electrolytes are present. Equation (3-2) is assumed to have a negatively solid matrix.

3.1.2 Constitutive Equations

For an isotropic hydrated charged mixture with infinitesimal deformation, the constitutive equations of triphasic theory are summarized below (45):

$$\text{Solid phase: } \boldsymbol{\sigma} = -p\mathbf{I} - T_c \boldsymbol{I} + \lambda_s e\mathbf{I} + 2\mu_s \mathbf{E} \tag{3-3}$$

$$\text{Fluid Phase: } \mu^w = \mu_0^w + \frac{[p - RT\phi(c^+ + c^-) + B_W e]}{\rho_T^w} \tag{3-4}$$

$$\text{Cation: } \mu^{+} = \mu_0^{+} + \left(\frac{RT}{M_{+}}\right)\ln(\gamma_{+}c^{+}) + \frac{F_c\psi}{M_{+}} \tag{3-5}$$

$$\text{Anion: } \mu^{-} = \mu_0^{-} + \left(\frac{RT}{M_{-}}\right)\ln(\gamma_{-}c^{-}) - \frac{F_c\psi}{M_{-}} \tag{3-6}$$

$$\text{Neutral Solute: } \mu^{\alpha} = \mu_0^{\alpha} + \left(\frac{RT}{M_{\alpha}}\right)\ln(\gamma_{\alpha}c^{\alpha}) \tag{3-7}$$

In Equation (3-3), p is fluid pressure, T_c is the chemical expansion stress that is a function of ion concentration, λ_s and $\mu_s$are the Lame coefficients of the solid matrix, e is the trace of the strain tensor **E**:

$$\mathbf{E} = \frac{1}{2}\left(\nabla \boldsymbol{u} + \nabla \boldsymbol{u}^{T}\right) \tag{3-8}$$

where $\boldsymbol{u}$ is the displacement of the solid matrix.

In Equations (3-4) to (3-7), μ^{β} is the reference chemical potential of the species (β= fluid phase w,+,-, α), R is the universal gas constant, T is the absolute temperature, ψ is the electrical potential, ϕ is the osmotic coefficient, $\gamma_{(+,-,\alpha)}$ is the activity coefficient of the cation, anion, and neutral solute, respectively, and B_w is the inter-phase coupling coefficient.

The modified electrochemical/chemical potential functions for fluid (w), Na^+, Cl^-, and neutral solutes are related to fluid pressure (p), electrical potential (ψ), and solute concentration (c^+, c^-, c^{α}), according to Sun et al. (1999) (45):

$$\text{Fluid phase: } \varepsilon^{w} = \frac{\rho_T^{W}(\mu^{W} - \mu_0^{W})}{\mathrm{RT}} = \frac{\mathrm{p}}{\mathrm{RT}} - \phi(\mathrm{c}^{+} + c^{-}) + \frac{B_W}{RT}e \tag{3-9}$$

$$\text{Cation}: \varepsilon^{+} = \gamma_{+}c^{+}e^{F_C\varphi/RT} \tag{3-10}$$

$$\text{Anion}: \varepsilon^{-} = \gamma_{-}c^{-}e^{F_C\varphi/RT} \tag{3-11}$$

$$\text{Neutral}: \varepsilon^{\alpha} = \gamma_{\alpha}c^{\alpha} \tag{3-12}$$

where e is the dilatation, F_c is the Faraday constant, ε^w, ε^+, and ε^- have a dimension of ion concentration. ε^α is the neutral solute concentration (α = ATP, ADP, AMP). Assume $B_w = 0$, $\psi = 0$ and $\gamma_{(+,-,\alpha)} = 1$ in this model.

The five primary Degrees of Freedom (DOFs) of the whole system are ε^w, ε^+, ε^-, ε^α and solid displacement u^s.

The governing equations include the balance of linear momentum for the mixture:

$$\nabla \cdot \sigma = 0 \tag{3-13}$$

The continuity equation of the mixture and ions are (36, 38, 45):

$$\nabla \cdot (v^s + J^W) = 0 \tag{3-14}$$

$$\frac{\partial(\phi^W c^+)}{\partial t} + \nabla \cdot (J^+ + \phi^w c^+ v^s) = 0 \tag{3-15}$$

$$\frac{\partial(\phi^W c^-)}{\partial t} + \nabla \cdot (J^- + \phi^w c^- v^s) = 0 \tag{3-16}$$

where σ is the total stress of the mixture, v^s is the velocity of the solid phase, J^β is the molar flux of the solute phase (β = w, +, -) relative to the solid phase, ϕ^W is the tissue porosity defined as the ratio of water volume to total tissue volume, and c^β is the concentration (β = w, +, -). The continuity equation for neutral solutes in this model is:

$$\frac{\partial(\phi^W c^\alpha)}{\partial t} + \nabla \cdot (J^\alpha + \phi^w c^\alpha v^s) = \mathrm{R}^\alpha \tag{3-17}$$

where ϕ^W is the osmotic coefficient of water, c^α is the concentration of neutral solute (α = ATP, ADP, AMP), J^α is the molar flux of neutral solutes, and R^α is the hydrolysis or production rate of neutral solute. The continuity equation for neutral solutes follows the conservation of mass for each component in the mixture (Equation 3-17).

3.1.3 Michaelis-Menten Equations

Michaelis-Menten equations were incorporated into multiphasic theory to analyze hydrolysis of ATP and its adenine derivatives in the IVD. Reactions governing hydrolysis of adenine derivatives are stated below:

$$(1)\ \mathrm{ATP} \rightarrow \mathrm{ADP} + \mathrm{P_i} \tag{3-18}$$

$$(2)\ \mathrm{ADP} \rightarrow \mathrm{AMP} + \mathrm{P_i} \tag{3-19}$$

$$(3)\ \mathrm{AMP} \rightarrow \mathrm{Adenosine} + \mathrm{P_i} \tag{3-20}$$

$$(4)\ \mathrm{ATP} \rightarrow \mathrm{AMP} + \mathrm{PP_i} \tag{3-21}$$

Only one enzyme was assumed to catalyze each reaction for ATP, ADP, AMP, and other products. The following Michaelis-Menten equations were used to describe the kinetics of ATP hydrolysis:

$$\mathrm{R}^{ATP} = J_{ATP} - \frac{V_1\, \mathrm{c}^{ATP}}{K_1 + \mathrm{c}^{ATP}} - \frac{V_4\, \mathrm{c}^{ATP}}{\mathrm{K}_4 + \mathrm{c}^{ATP}} \tag{3-22}$$

$$\mathrm{R}^{ADP} = \frac{V_1\, \mathrm{c}^{ATP}}{K_1 + \mathrm{c}^{ATP}} - \frac{V_2\, \mathrm{c}^{ADP}}{\mathrm{K}_2 + \mathrm{c}^{ADP}} \tag{3-23}$$

$$R^{AMP} = \frac{V_2\, \mathrm{c}^{ADP}}{K_2 + \mathrm{c}^{ADP}} + \frac{V_4\, \mathrm{c}^{ATP}}{\mathrm{K}_4 + \mathrm{c}^{ATP}} - \frac{V_3\, c^{AMP}}{\mathrm{K}_3 + c^{AMP}} \tag{3-24}$$

where c^{α} is the solute concentration (α = ATP, ADP, AMP), V_i and K_i are the maximum reaction velocity and Michaelis constant (i =1, 2, 3, 4), respectively, and J_{ATP} is the ATP release rate. The Michaelis-Menten parameters V_i and K_i in Equations (3-22) to (3-24) are numbered to correspond to Equations (3-18) to (3-21).

Governing equations in multiphasic theory follow the balance of linear momentum for the mixture and the conservation of mass for each phase. Tissue porosity and diffusivity

are several strain-dependent tissue properties in the model, which are critical parameters to consider when mechanical loading applies compressive strain on the tissue. Strain-dependent permeability can limit the rate of stress transfer from fluid to the solid matrix (46).

The flux for neutral solutes, Na^+, and Cl^- are:

$$\text{Neutral: } J_r^{\alpha} = H^0 c_r^{\alpha} J_r^{w} - \frac{D^{\alpha}}{H_A k_0} \frac{\phi^w c_r^{\alpha}}{\varepsilon_r^{\alpha}} \nabla_r \varepsilon_r^{\alpha} \tag{3-25}$$

$$\text{Cation: } J_r^{+} = H^0 c_r^{+} J_r^{w} - \frac{D^{+}}{H_A k_0} \frac{\phi^w c_r^{+}}{\varepsilon_r^{+}} \nabla_r \varepsilon_r^{+} \tag{3-26}$$

$$\text{Anion: } J_r^{-} = H^0 c_r^{-} J_r^{w} - \frac{D^{-}}{H_A k_0} \frac{\phi^w c_r^{-}}{\varepsilon_r^{-}} \nabla_r \varepsilon_r^{-} \tag{3-27}$$

where H^0 is the hindrance factor of the solute for convection, H_A is the aggregate modulus, k_0 is the basic scale of permeability, ϕ^w is the tissue porosity, and ε_r^{α} is the electrochemical potential of the solute. The convective and diffusive fluxes are represented in Equations (3-25) to (3-27).

The hydrodynamic radius, r_s, of each solute was calculated based on the Stokes-Einstein equation (Table 3-1):

$$D_0 = \frac{k_b T}{6 \pi \eta r_s} \tag{3-28}$$

where r_s is the hydrodynamic radius, k_b is the Boltzmann constant, T is the temperature, η is the solvent viscosity, and D_0 is the diffusivity of the neutral solute in aqueous solution at 37°C (α = ATP, ADP, AMP). The equation can be solved in terms of r_s, also known as the Stokes radius.

Table 3-1: Diffusivities of neutral solutes

Solute	D_0 (m^2/s)	r_s (nm)
ATP	2.60×10^{-10}	0.981
ADP	3.09×10^{-10}	0.825
AMP	3.80×10^{-10}	0.671

Next, the hydrodynamic radius was used to estimate diffusivity and permeability of each solute. The hydraulic permeability k of the tissue was calculated based on the following constitutive equation (47):

$$k = a * (\frac{\phi^w}{1-\phi^w})^n \tag{3-29}$$

where $a = 0.00339$ and $n = 0.24$. The material constants a and n were previously determined for agarose gels and cartilaginous tissue (47).

The dependence of solute diffusivity (D^α) on the tissue porosity is estimated by the following constitutive relationship derived by Gu et al. (2004) (48):

$$\frac{D^\alpha}{D_0^\infty} = \exp\left[-(A)*\left(\frac{r_s}{\sqrt{k}}\right)^B\right] \tag{3-30}$$

where A = 1.25, B = 0.681, D_0^∞ is the diffusivity of the solute in aqueous solution, and k is the hydraulic permeability of the porous medium. The material constants, A and B, depend on the type of tissue and were previously determined for agarose gels and the IVD.

Tissue porosity (ϕ^w) is related to tissue dilatation, e, and the porosity at the reference configuration (i.e. at e = 0), in the following equation:

$$\phi^w = \frac{\phi_0^w + e}{1+e} \tag{3-31}$$

where ϕ_0^w is the interstitial fluid volume fraction at the reference configuration.

The reference configuration is the hypertonic state, corresponding to infinite salt concentration. Therefore, in this model, intrinsic solute diffusivities and permeabilities are all strain-dependent tissue properties.

3.2 Experimental Determination of V_1 and K_1 for Extracellular ATP Hydrolysis

Michaelis-Menten parameters for V_1 and K_1 of extracellular ATP hydrolysis have not yet been measured in the IVD. Thus, experimental values were determined and implemented into the theoretical model. The experimental method is described next.

IVD cells were first isolated from porcine lumbar discs. Adult pigs were obtained from a local slaughter house and dissected approximately within 2 h of sacrifice. The spines were extracted using bone cutting forceps and surgical scalpels. After removing excess tissue around the spine, they were rinsed in phosphate-buffered saline (PBS) containing 10% antibiotic-antimycotic (Invitrogen Corp.) several times. Then the spines were moved to a biological safety cabinet for dissection. To open each disc, a scalpel was cut through the center of the outer AF to the inner NF region. Discs were exposed by making a transverse cut on either the superior or inferior margin. Then NP and outer AF tissues were carefully harvested from the discs without removing the endplate. Outer AF tissue and inner NP tissue were independently isolated using scalpels and tweezers, respectively. AF tissue was finely chopped to expedite tissue digestion. Cells were released from AF and NP tissues by enzyme digestion in high glucose (25 mmol/L) Dulbecco's Modified Eagle Medium (DMEM; Invitrogen Corp., Carlsbad, CA) supplemented with 10% fetal bovine serum (FBS; Invitrogen Corp.) and 1% antibiotic-antimycotic (Invitrogen Corp.) for 24 hours. The enzyme solution contained 0.5 mg/mL collagenase and 0.3 mg/mL protease for NP and AF tissues. After the digestions were filtered by a sterile 70-μm cell strainer (BD

Biosciences, Bedford, MA), cells were recovered by centrifugation and then resuspended in high-glucose DMEM containing 10% FBS and 1% antibiotic-antimycotic.

Next, cells were encapsulated in 2% agarose discs (8 mm in diameter, 1 mm thick) at a density of $1x10^6$ cells/disc. Three-dimensional agarose culture has been reported to maintain the phenotype of IVD cells (49). The agarose discs were plated in high-glucose DMEM containing 10% FBS and 1% antibiotic-antimycotic at 37°C.

For NP and AF cells, two different concentrations of ATP were injected into custom-made chambers. A range of ATP concentrations were tested to find the optimal concentration for each cell type. First, a 1 mM ATP stock solution made from lyophilized ATP sodium salt hydrate (Sigma) was diluted in serum-free DMEM to the desired concentration that resulted in an ATP concentration that is hydrolyzed by the IVD cell nearly to zero at t = 4 hr, i.e. 10 μM for NP cells and 150 μM for AF cells. Next, it was sterile filtered and mixed with the appropriate volume of serum-free DMEM, 600 μL of media overall, in an Eppendorf tube to produce the desired ATP concentration. Then the medium was transferred to the chamber.

Next, the cell-agarose disc was cut into small pieces on a clean glass slide, about 1 mm cubes, to minimize the concentration gradient of oxygen within the agarose gel. Then it was added to the chamber filled with 600 μL of serum-free DMEM and ATP. It was placed on the magnetic stirrer for 5 minutes to facilitate cellular adaptation to the new medium (Figure 3-1). Then the chamber was placed inside an incubator at 37°C in 5% CO_2. The negative control consisted of an agarose disc placed into a chamber with serum-free DMEM without ATP injection. Three sample chambers (n = 3) were prepared to mitigate sample-to-sample variability.

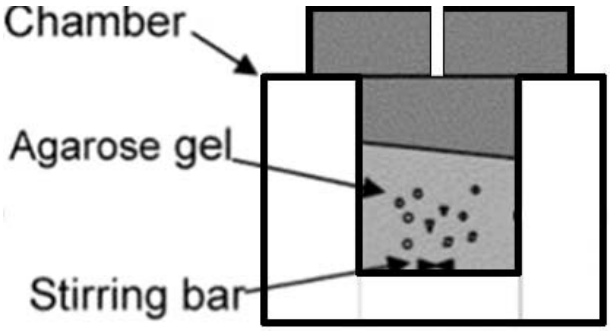

Figure 3-1: Schematic of ATP hydrolysis experiment. 600 µL of serum-free DMEM and ATP were added to a chamber. The agarose disc was cut into small cubes, and a stirring bar was placed into the chamber to create a homogenous mixture.

At each time point (1/12 h, 1 h, 2 h, 3 h, 4 h), 5 µL of media was removed every hour and diluted in 95 µL DMEM (1:20 dilution). A small volume was chosen because a lack of normalization would be justified when the vast majority of the original media volume was present at the end of the assay (95.8%). Then a 1:1 ratio of ATP stabilizing solution was added (1:40 dilution overall). Samples were boiled for 2 min to release ATP into the culture media. All samples were stored at -80°C until they were tested using the ATP bioluminescence assay.

For the ATP bioluminescence assay, extracellular ATP measurements were performed using the Luciferin-luciferase method (Sigma) (50) (51). Serum-free DMEM was used to prepare a standard curve, which is a linear curve created from standard concentrations. Since FBS may contain nucleotidase activity that can hydrolyze ATP, only DMEM without any supplements could be used (52). When necessary, extracellular ATP samples were diluted in serum-free DMEM to lower the luminescence value to the range

of the standard curve, 10 nM to 100 nM. The final concentration was calculated from the standard curve that provided a conversion factor between concentration and luminescence.

Next, experimental data of ATP concentrations were calculated and plotted against time. The Michaelis-Menten equation describing the association between ATP hydrolysis rate and ATP concentration is (6):

$$\frac{dC}{dt} = -R_0 = -\frac{V_{\max} C}{K_M + C}\rho \tag{3-32}$$

where R_0 is the solute hydrolysis rate, t is time, C is the solute concentration and ρ is the cell density.

The analytical solution of the governing equation (3-32) is:

$$t = \frac{K_M}{V_{max}\,\rho}\ln\frac{C_0}{C} + \frac{C_0 - C}{V_{max}\,\rho} + t_0 \tag{3-33}$$

where C_0 is the initial concentration of solute at the initial time point t_0. Then Michaelis-Menten parameters V_1 and K_1 were determined by curve fitting of experimental data with Equation (3-33) using MATLAB (Mathworks, Natick, MA).

3.3.1 Numerical Implementation of Finite Element Analysis

A finite element method (FEM) formulation is constructed using the standard Galerkin weighted residual method. A Newton-Raphson iterative procedure is used to calculate nonlinear terms in the equations. The FEM formulation, employing the weak form, was developed by Sun et al. (1999) and is given by (45):

$$\int_\Omega \mathbf{w}\cdot\nabla\cdot\sigma \; d\Omega = 0 \tag{3-34}$$

$$\int_\Omega w^{(1)}[\nabla\cdot(\mathbf{v}^s + \mathbf{J}^{\mathrm{W}})] \; d\Omega = 0 \tag{3-35}$$

$$\int_\Omega w^{(2)}[\frac{\partial(\phi^W c^+)}{\partial t} + \nabla\cdot(J^+ + \phi^W c^+ \mathbf{v}^{\mathbf{s}})]\, d\Omega = 0 \tag{3-36}$$

$$\int_\Omega w^{(3)}[\frac{\partial(\phi^W c^-)}{\partial t} + \nabla \cdot (J^- + \phi^W c^- \mathbf{v^s})]\, d\Omega = 0 \quad (3\text{-}37)$$

$$\int_\Omega w^{(4)}[\frac{\partial(\phi^W c^\alpha)}{\partial t} + \nabla \cdot (J^\alpha + \phi^W c^\alpha \mathbf{v^s}) - R^\alpha]\, d\Omega = 0 \quad (3\text{-}38)$$

where the vector **w** and scalar functions $w^{(1)}$, $w^{(2)}$, $w^{(3)}$, $w^{(4)}$ are arbitrary admissible weighting functions for the governing equations.

The weak formulation of multiphasic theory after applying divergence theorem is:

$$\int_\Omega \mathrm{tr}[\,(\nabla \mathbf{w})^T \cdot \sigma]\, d\Omega = \int_\Gamma \mathbf{w} \cdot \mathbf{t}^*\, d\Gamma \quad (3\text{-}39)$$

$$\int_\Omega w^{(1)} \nabla \cdot \mathbf{v^s}\, d\Omega - \int_\Omega \mathbf{J^W} \cdot \nabla w^{(1)} d\Omega = -\int_{\Gamma_{\mathbf{Jw}}} w^{(1)} \mathbf{J^{w*}} \cdot \mathbf{n}\, d\Gamma \quad (3\text{-}40)$$

$$\int_\Omega w^{(2)} \frac{\partial(\phi^W c^+)}{\partial t}\, d\Omega - \int_\Omega \mathbf{J^+} \cdot \nabla w^{(2)} d\Omega + \int_\Omega w^{(2)} \nabla \cdot (\phi^W c^+ \mathbf{v^s})\, d\Omega =$$

$$-\int_{\Gamma_{\mathbf{J}+}} w^{(2)} \mathbf{J^{+*}} \cdot \mathbf{n}\, d\Gamma \quad (3\text{-}41)$$

$$\int_\Omega w^{(3)} \frac{\partial(\phi^W c^-)}{\partial t}\, d\Omega - \int_\Omega \mathbf{J^-} \cdot \nabla w^{(3)} d\Omega + \int_\Omega w^{(3)} \nabla \cdot (\phi^W c^- \mathbf{v^s})\, d\Omega =$$

$$-\int_{\Gamma_{\mathbf{J}-}} w^{(3)} \mathbf{J^{-*}} \cdot \mathbf{n}\, d\Gamma \quad (3\text{-}42)$$

$$\int_\Omega w^{(4)} \frac{\partial(\phi^W c^\alpha)}{\partial t}\, d\Omega - \int_\Omega \mathbf{J^\alpha} \cdot \nabla w^{(4)} d\Omega + \int_\Omega w^{(4)} \nabla \cdot (\phi^W c^\alpha \mathbf{v^s})\, d\Omega - \int_\Omega w^{(4)} R^\alpha d\Omega =$$

$$-\int_{\Gamma_{\mathbf{J}^\alpha}} w^{(4)} \mathbf{J^{\alpha*}} \cdot \mathbf{n}\, d\Gamma \quad (3\text{-}43)$$

where w is the arbitrary weighting function and t* is the traction on the boundary of the tissue and * represents quantities on the tissue boundary.

Using the finite element software COMSOL (COMSOL, 4.3a, Burlington, MA), a two-dimensional model of the IVD was assumed to be axisymmetric with the geometry only representing the top right quadrant of the disc (Figure 3-2). It was modeled with a mesh composed of 584 quadrilateral elements (Figure 3-3).

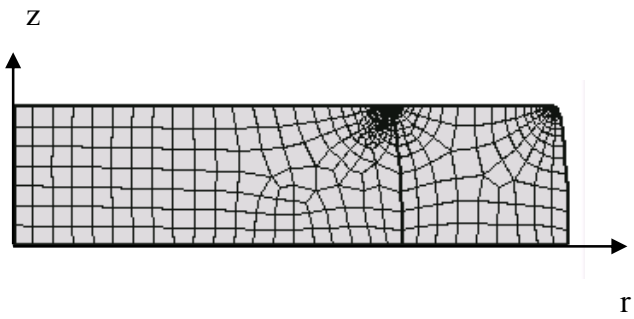

Figure 3-2: Computational domain of IVD. Geometrical symmetry of the disc justifies modeling of only the top right quadrant of the IVD. The finite element model is assumed to be axisymmetric.

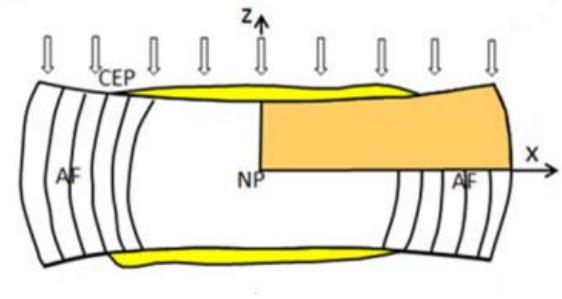

Figure 3-3: Schematic of upper right quadrant of IVD. The IVD is assumed to be axisymmetric in the finite element model (43).

The convergence criterion was a relative error tolerance of less than 10^{-6}. Three neutral solutes (ATP, ADP, AMP), sodium (Na^+), and chloride (Cl^-) were considered in this model. ATP and its adenine derivatives are assumed to exhibit no coupling effect with these ions. Charged ions are necessary for balancing the fixed negative charge on the solid matrix. Michaelis-Menten parameters were normalized with respect to the solute concentration, which corresponds to the blood supply at the AF edge of the IVD, (Table 3-2) (53, 54).

The AMP concentration in the blood supply is not reported in the literature, but it is estimated to be approximately equal to the ADP concentration. Nondimensionalization also converts parameters to unitless quantities to make relative comparisons possible between different solutes.

Table 3-2: Plasma concentration of ATP, ADP, and AMP for normalization

Solute	**Plasma Concentration (μM)**
ATP (53)	1
ADP (54)	0.13
AMP*	0.13*

*The AMP plasma concentration is not reported in the literature, but it is estimated to be nearly equal to ADP concentration.

The following are definitions of the major non-dimensional quantities:

$$\hat{t} = \frac{t}{h_0^2 / H_A^* k_0}, \hat{c}^{\alpha} = \frac{c^{\alpha}}{c^{\alpha *}}, \hat{V}_{\max} = \frac{V_{\max}}{c^{\alpha *} * h_0^2 / H_A^* k_0}, \hat{K}_M = \frac{K_M}{c^{\alpha *}} \qquad (3\text{-}44)$$

where k_0 is the reference permeability, which was chosen to be 5 x 10^{-16} m^4/Ns, H_A^* is the reference equilibrium modulus, and $c^{\alpha *}$ is the reference concentration of the neutral solute (α = ATP, ADP, and AMP).

3.3.2 Boundary Conditions

The symmetry of the computational domain results in the following boundary conditions (Table 3-3):

Table 3-3: Specific boundary conditions of finite element analysis

At the AF edge (lateral surface of AF)

$$c^{Cl^-} = c^{Na^+} = 0.15\,M$$
$$c^{ATP} = 1\,\mu M$$
$$c^{ADP} = c^{AMP} = 0.13\mu M$$

At the mid-height (z = 0)

$$J_z^{water} = J_z^{Na^+} = J_z^{Cl^-} = J_z^{ATP} = 0$$
$$u_z = 0, \sigma_{rz} = 0$$

At the disc center (r = 0)

$$J_z^{water} = J_z^{Na^+} = J_z^{Cl^-} = J_z^{ATP} = 0$$
$$u_z = 0, \sigma_{zr} = 0$$

At endplate (z = h)

$$J_z^{water} = J_z^{Na^+} = J_z^{Cl^-} = J_z^{ATP} = 0$$
$$c^{Cl^-} = c^{Na^+} = 0.15\,M$$
$$u_r = u_z = 0$$

$u_z = 0$	no compression
$u_z = -u_0$	under static compression
$u_z = -u_0 - u_1 \sin(2\pi ft)$	under dynamic compression

3.3.3 Determination of V_{max} and K_M Based on Chondrocytes

In the literature, Michaelis-Menten parameters for hydrolysis of ADP and AMP (V_2, K_2, V_3, K_3) were not available for the IVD. Since AF were considered to be metabolically similar to chondrocytes, these parameters were derived from hydrolysis data of ADP and AMP in a previous chondrocyte study by Hatori et al. (1995) (55). The theoretical curve fitting was performed on experimental data with Equation (3-33) using

MATLAB (Mathworks, Natick, MA) to yield V_{max} and K_M for the hydrolysis of ADP and AMP (55).

3.3.4 Dynamic Compression and Implementation of Experimental Data

Next, V_1 and K_1 values calculated from the ATP hydrolysis experiment were implemented into the theoretical model (Table 3-4). Michaelis-Menten parameters for adenine derivatives (ADP, AMP) were derived from Hatori et al. (1995) (55). Then parametric analysis was performed to evaluate the value of J_{ATP} based on the extracellular ATP accumulation (i.e. 166 µM) observed by Wang et al. (2013) (9).

Table 3-4: Parameters used for dynamic compression. Experimental data for V_1 and K_1 were input into the theoretical model. Data for V_2 and V_3 were derived from Hatori et al. (1995).

Parameter	Value	Source
$V_{1, NP}$	0.00659 mmol/sec*m^3	Current study
$V_{1, AF}$	0.0143 mmol/sec*m^3	Current study
$V_{2, NP}$	2.4 X 10^{-2} mmol/sec*m^3	Hatori et al. (1995)
$V_{2, AF}$	5.4 X 10^{-2} mmol/sec*m^3	Hatori et al. (1995)
$V_{3, NP}$	3.72 X 10^4 mmol/sec*m^3	Hatori et al. (1995)
$V_{3, AF}$	8.37 x 10^4 mmol/sec*m^3	Hatori et al. (1995)
$K_{1, AF}$	14.144 µM	Current study
$K_{1, NP}$	3.925 µM	Current study
K_2	38 µM	Hatori et al. (1995)
K_3	2.26 X 10^4 µM	Hatori et al. (1995)

Numerical analysis of dynamic compression was incorporated into the model to simulate daily physical loading, which could predict changes in extracellular ATP distribution during mechanical compression. Then the transport and distribution of

extracellular ATP in the IVD under three loading configurations were analyzed: no compression, static compression, dynamic compression (Figure 3-4). First, the IVD was subject to prescribed boundary conditions without compression. During static compression, the disc was compressed between two endplates with a constant displacement until equilibrium was reached. The initial strain was 10%. For dynamic compression, the equilibrium state of static compression was used as the initial condition, and then the disc was compressed with a sinusoidal displacement with a strain of 5% and frequency f = 0.05 Hz. The number of time steps per cycle was 10. The endplate region adjacent to the AF was assumed to be calcified, so it was modeled as impermeable to solutes. A mesh of 584 second-order quadrilateral elements was used to analyze the two-dimensional model of the disc.

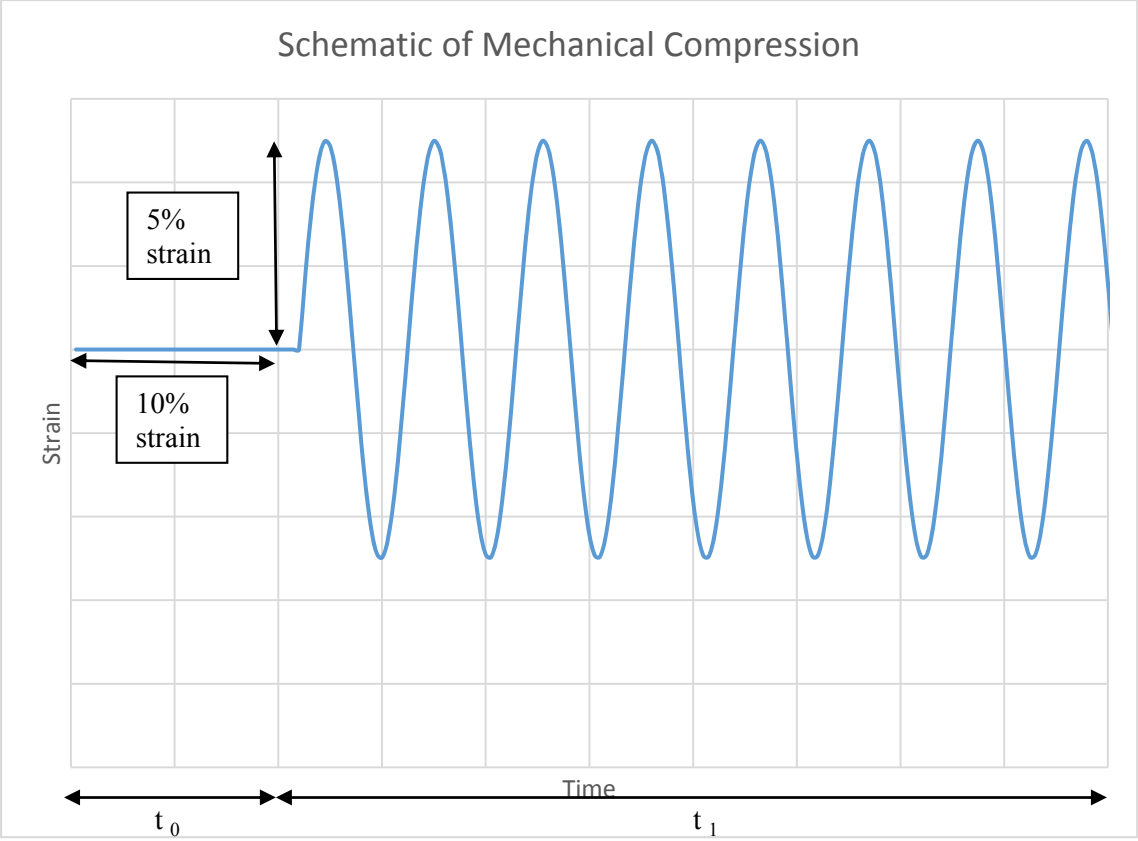

Figure 3-4: Displacement boundary condition for dynamic compression of the IVD. An initial strain of 10% was applied for the static case ($t = t_0$), and a sinusoidal function with 5% strain was applied for the dynamic case. For dynamic compression ($t = t_1$), 360 cycles were run and each cycle was 20 s for a total time of 2 hr.

Chapter 4—Results

4.1 Michaelis-Menten Parameters of IVD Cells

The value of Michaelis-Menten parameters, V_1 and K_1, differed significantly between NP and AF cells. Moreover, a significant difference in luminescence was observed between samples and negative control. The negative control resulted in negligible ATP concentration that remained relatively constant over 4 hours. ATP hydrolysis of NP and AF cells were measured using various concentrations of injected ATP, 10 μM for NP cells and 150 μM for AF cells. For NP cells, the optimal concentration was significantly lower than AF cells in order to result in an ATP hydrolysis rate with minimal ATP concentration at the last time point (Figure 4-1 and 4-2).

Experimental values of the Michaelis-Menten parameters for AF and NP cells were calculated. The mean value of V_1 for AF cells (n = 3) was 0.0143 ± 0.00990 mmol/s*m^3, and the mean V_1 for NP cells (n = 3) was 0.00659 ± 0.00677 mmol/s*m^3 (Figure 4-3 and 4-4). The mean value of K_1 for AF cells (n = 3) was 14.144 ± 9.452 μM, and the mean K_1 for NP cells (n = 3) was 3.925 ± 4.290 μM.

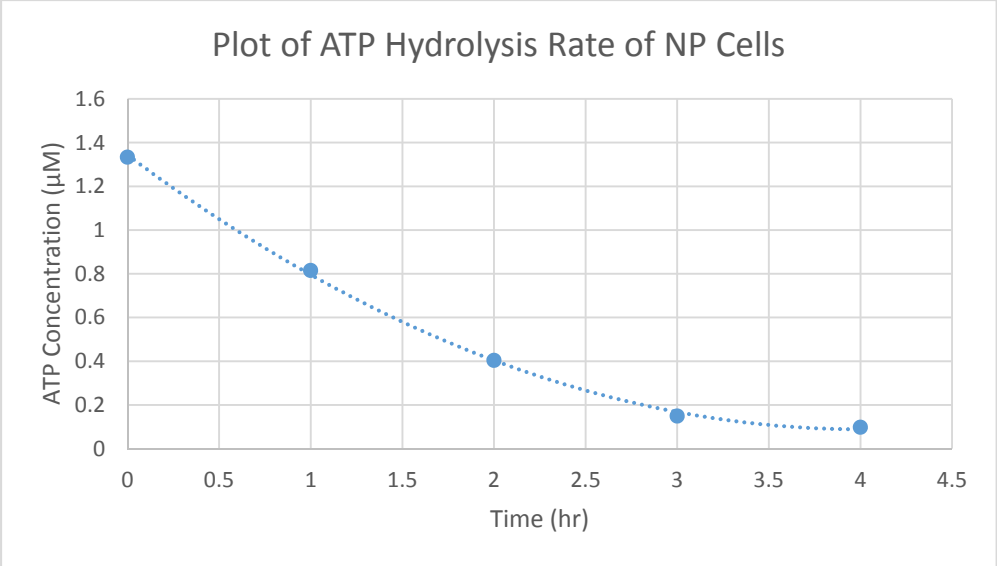

Figure 4-1: ATP hydrolysis experiment for NP cells. After 4 hours, nearly all extracellular ATP is hydrolyzed. Curve fitting was used to calculate V_1 and K_1.

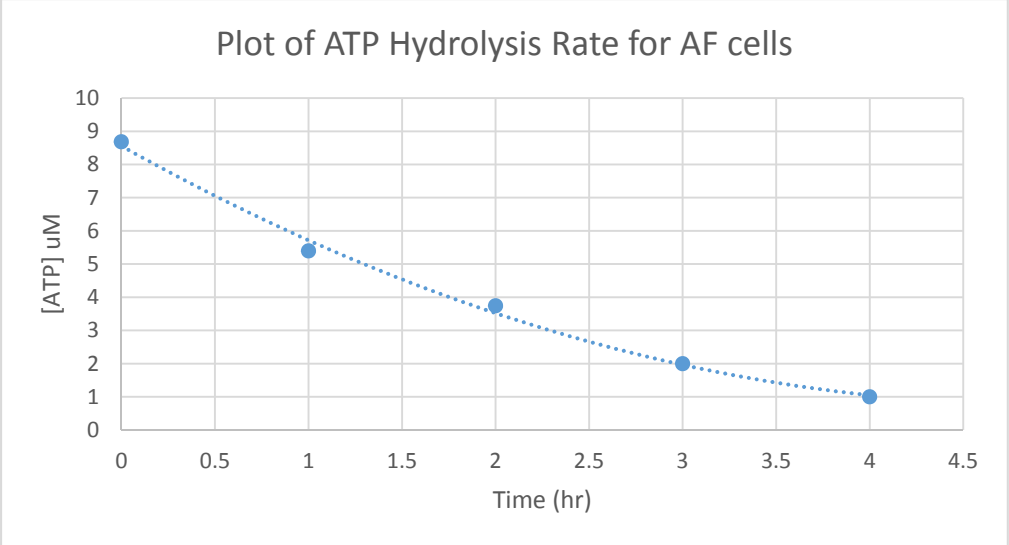

Figure 4-2. ATP hydrolysis experiment for AF cells. The result of the ATP hydrolysis experiment for AF cells shows that the V_1 for AF cells is greater than that of NP cells.

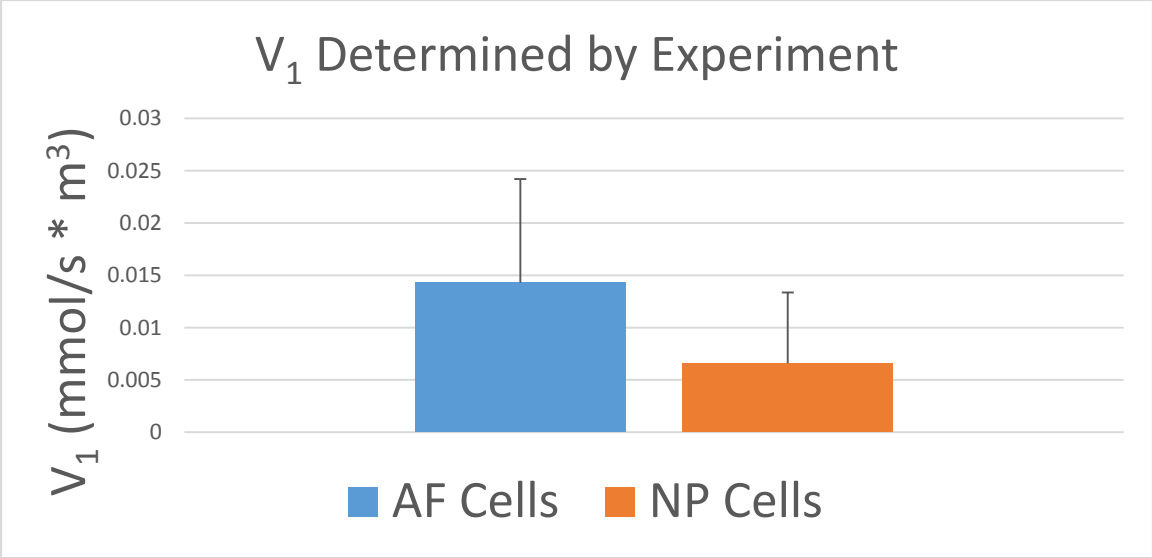

Figure 4-3: Data for V_1 from NP and AF cells in ATP hydrolysis experiment. V_1 is the maximum velocity of ATP and calculated by curve fitting, showing that the V_1 for AF cells is 53.9% higher than NP cells.

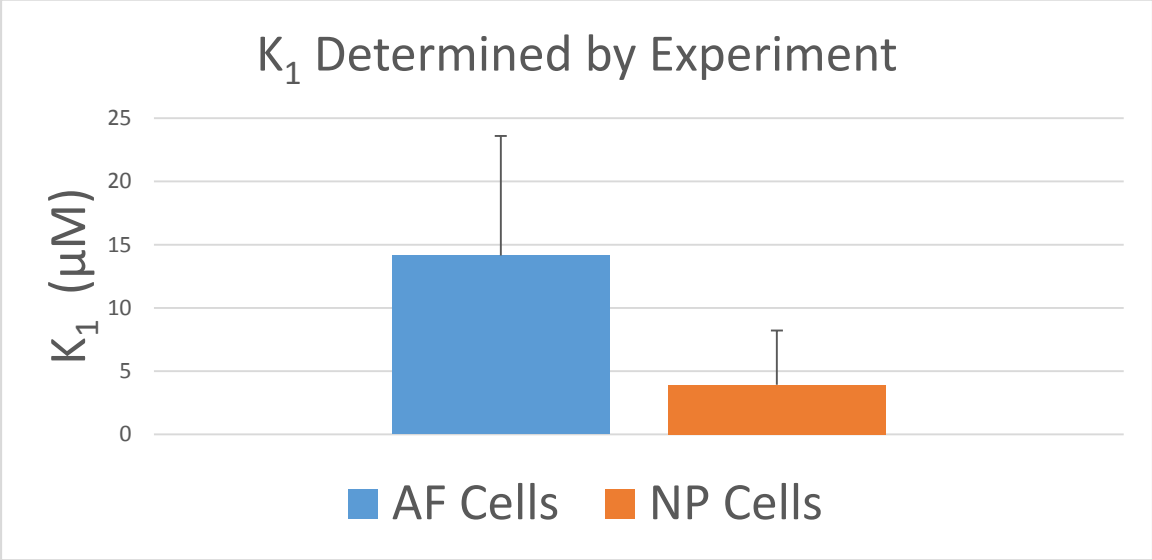

Figure 4-4: Data for K_1 from NP and AF cells in ATP hydrolysis experiment. K_1 is the Michaelis constant for ATP and is calculated by curve fitting.

4.2 Concentration of Extracellular ATP and Adenine Derivatives

Because data for the ATP release rate J_{ATP} in the IVD was unavailable in the literature, a parametric analysis was performed to evaluate J_{ATP}. J_{ATP} was assumed to be close to the value of V_1 (0.00659 mmol/sec*m^3). Three values of J_{ATP} (V_1, 2* V_1, 4 * V_1) were evaluated (Figure 4-1). With J_{ATP} = 2* V_1, the finite element model resulted in an extracellular ATP concentration accumulating to about 165 µM in the NP region and 10 µM in the AF region, which are comparable to the results reported in the study by Wang et al. (2013) (Figure 4-5). In the absence of mechanical loading, the maximum ADP concentration was 13.6 µM (Figure 4-7) and the maximum AMP concentration was 125.5 µM (Figure 4-8).

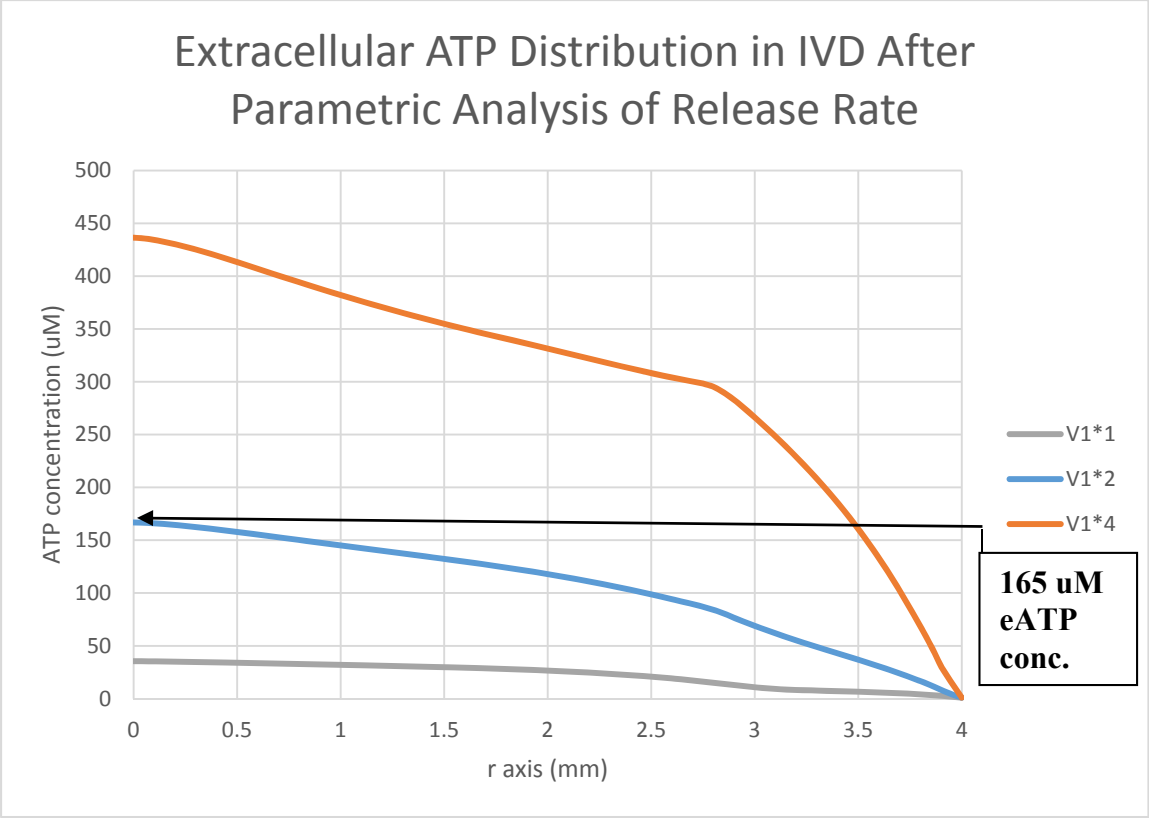

Figure 4-5: Parametric analysis of release rate J_{ATP} for extracellular ATP distribution. The extracellular ATP distribution after mechanical compression was plotted using different adjustment factors of J_{ATP}. The optimal J_{ATP} is about 2 times the original value to result in an ATP distribution that falls within the range measured by Wang et al. (2013). The concentration gradient of ATP along the r axis increases as J_{ATP} increases.

Using chondrocyte data from Hatori et al. (1995), V_{max} and K_M were calculated by theoretical curve fitting (Table 4-1). V_1 is the maximum velocity for the hydrolysis of ATP into ADP and P_i, and V_2 refers to ADP hydrolyzed to AMP and P_i, and V_3 refers to AMP hydrolyzed to adenosine and P_i.

Table 4-1: Curve fitting of chondrocyte data from Hatori et al. (1995) (55)

ATP V_1 =9.68 X 10^{-10} mmol/ s* million cells K_1 = 131.04 μM r^2 = 0.9998
ADP V_2 = 6 X 10^{-9} mmol/s*million cells K_2 = 38.0 μM r^2 = 0.978
AMP V_3 = 9.30 X 10^{-3} mmol/s*million cells K_3 = 2.26 X 10^4 μM r^2= 0.9981

The application of 10% strain during static compression did not significantly change the concentration of ATP or its adenine derivatives, but dynamic compression resulted in a concentration change. Dynamic compression at a frequency of 0.05 Hz for 2 hours was chosen to perform a theoretical simulation of a previous experiment by Wang et al. (2013) that measured changes in ATP concentration after mechanical loading on IVD cells (9). The theoretical model resulted in a 1.0% decrease in maximum ATP concentration, from 165.92 μM to 164.32 μM (Figure 4-6). The maximum concentration of ADP increased 0.2% from 13.60 μM to 13.63 μM (Figure 4-7), and the maximum AMP concentration increased 0.8% from 125.5 μM to 126.5 μM (Figure 4-8) after dynamic compression.

Next, a 50% increase in V_1 was chosen because Wang et al. (2013) observed an estimated 50% decrease in ATP concentration after static or dynamic compression compared to a control (Figure 4-8). This test could verify whether the theoretical model could also produce this result. For a 50% increase in V_1, the maximum concentration of

ATP decreased by 35.7% (Figure 4-12), the maximum concentration of ADP increased by 70.5% (Figure 4-13), and the maximum concentration of AMP increased by 42.2% (Figure 4-13). A smaller increase in V_1 was chosen to test the relationship between a change in solute concentration and increase in breakdown rate. Next, a 10% increase in V_1 was tested to find a relationship between change in V_1 and change in ATP concentration. For a 10% increase in V_1, the maximum concentration of ATP decreased by 7.6%, the maximum concentration of ADP increased by 13.3%, and the maximum concentration of AMP increased by 9.2%.

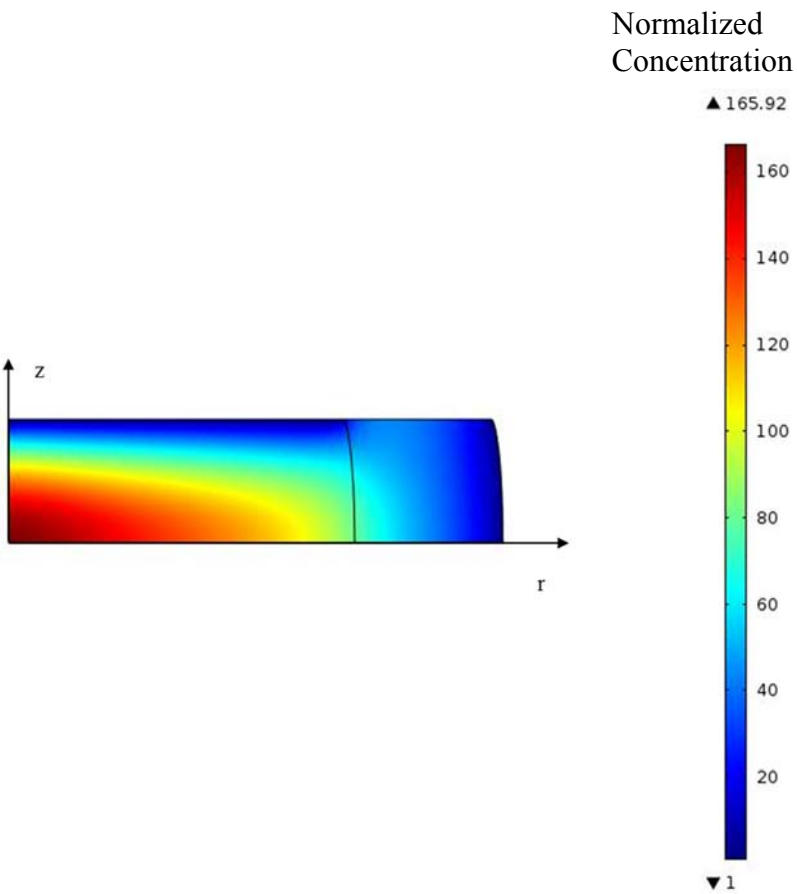

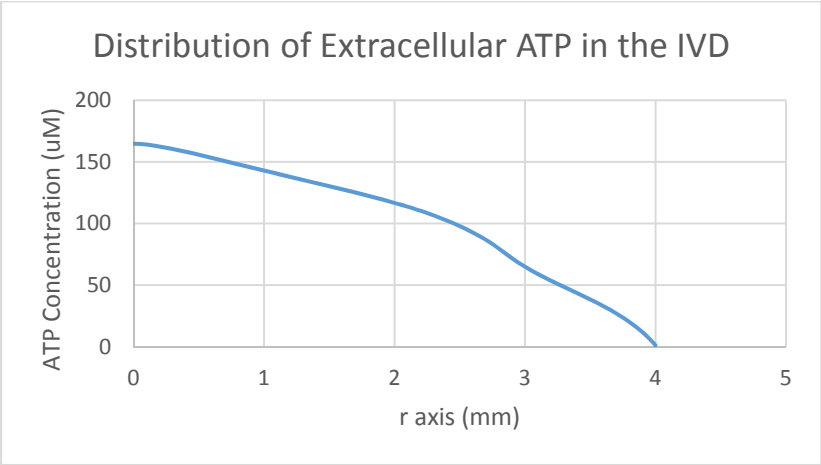

Figure 4-6: Image of extracellular ATP distribution. Experimental data was implemented into the theoretical model without mechanical load. No strain was applied to the disc. The maximum ATP concentration was about 166 μM at the center of the IVD.

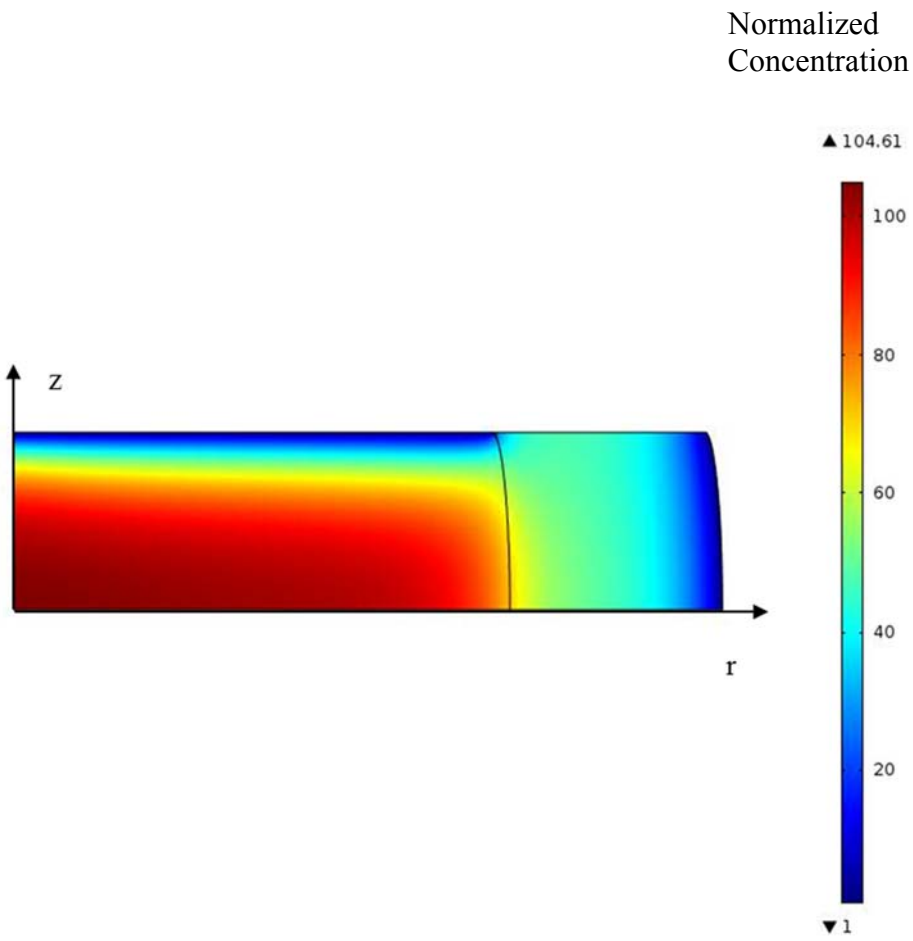

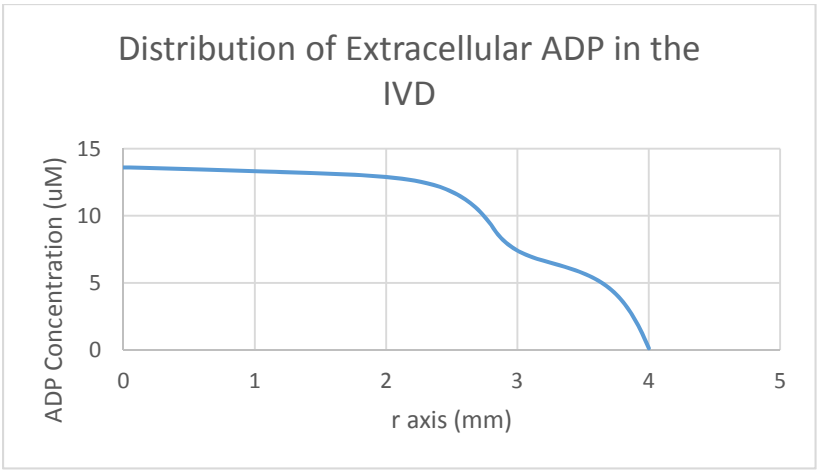

Figure 4-7: Image of extracellular ADP distribution. The ADP concentration was determined using curve fitting of chondrocyte data without mechanical loading. Values were normalized to the solute's concentration in the blood supply, resulting in a maximum ADP concentration of 13.6 μM.

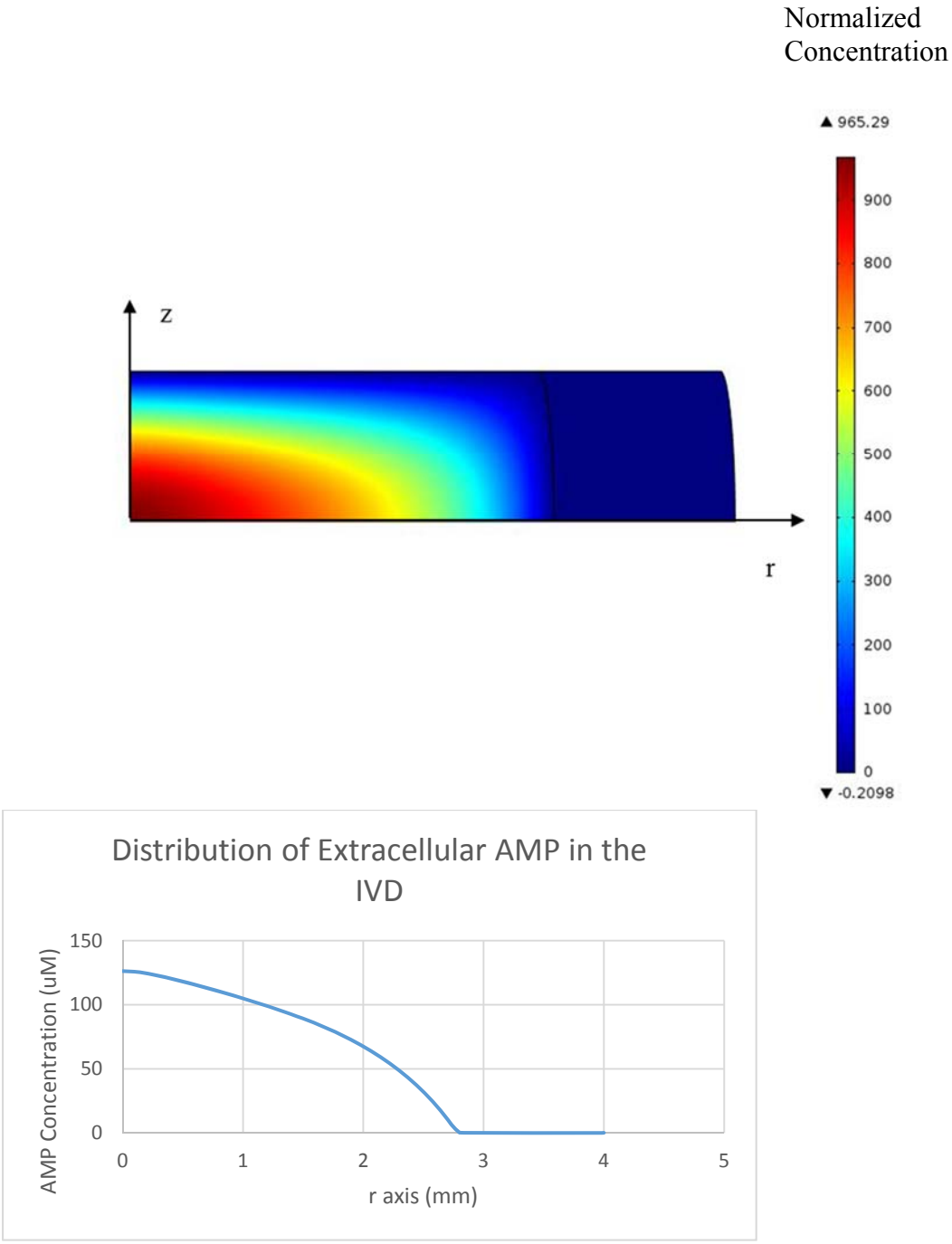

Figure 4-8: Image of extracellular AMP distribution. The AMP concentration was determined using curve fitting of chondrocyte data without mechanical load. Values were normalized to the solute's concentration in the blood supply, resulting in a maximum AMP concentration of 125.5 μM.

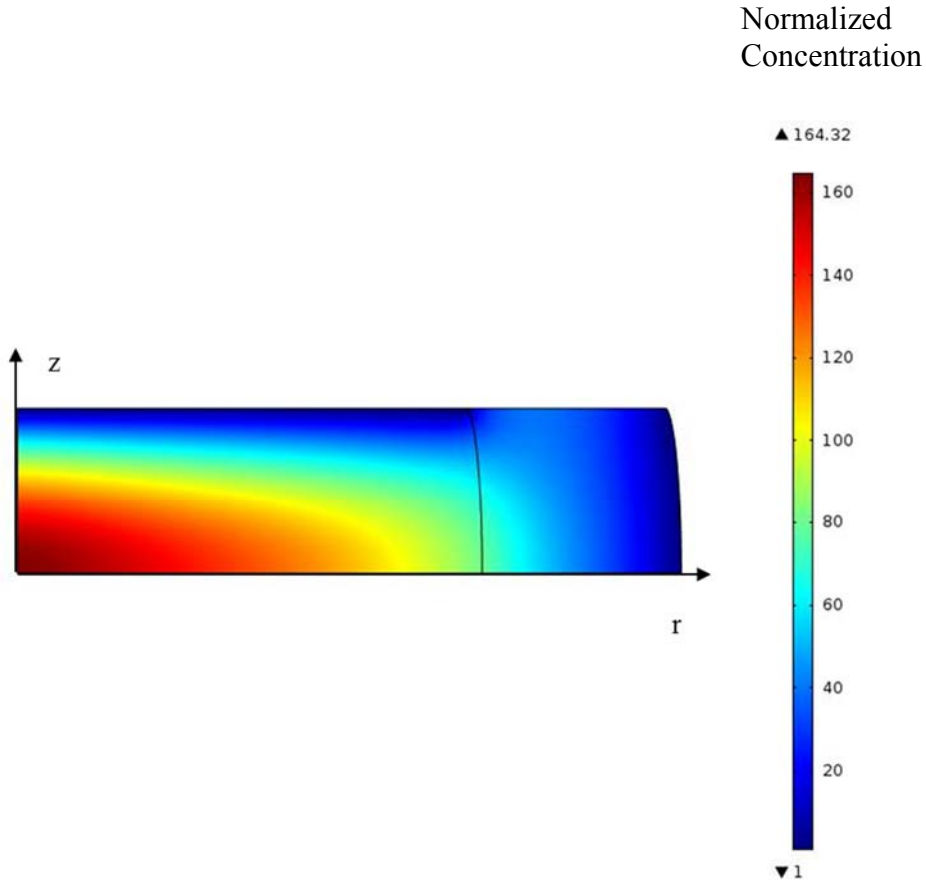

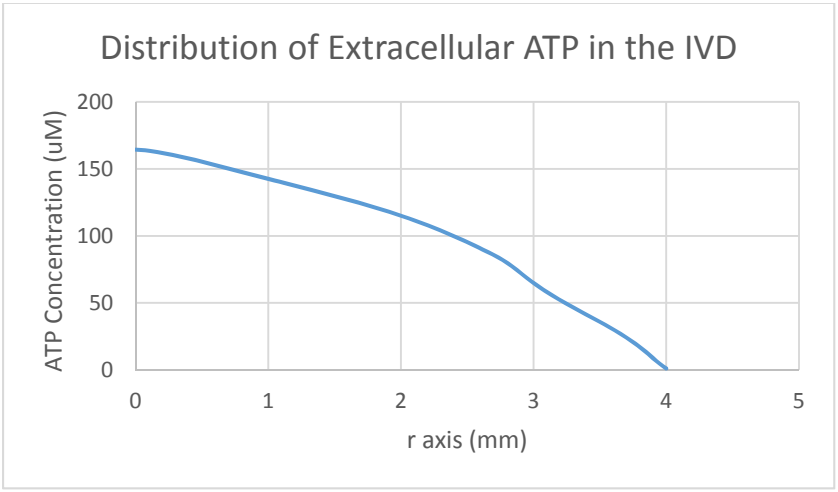

Figure 4-9: ATP concentration after dynamic compression. Dynamic compression was at frequency 0.05 Hz for t= 2 hr and resulted in a 1.0% decrease in ATP concentration. Boundary conditions were an initial strain of 10% for static compression and 5% strain with sinusoidal displacement for dynamic compression.

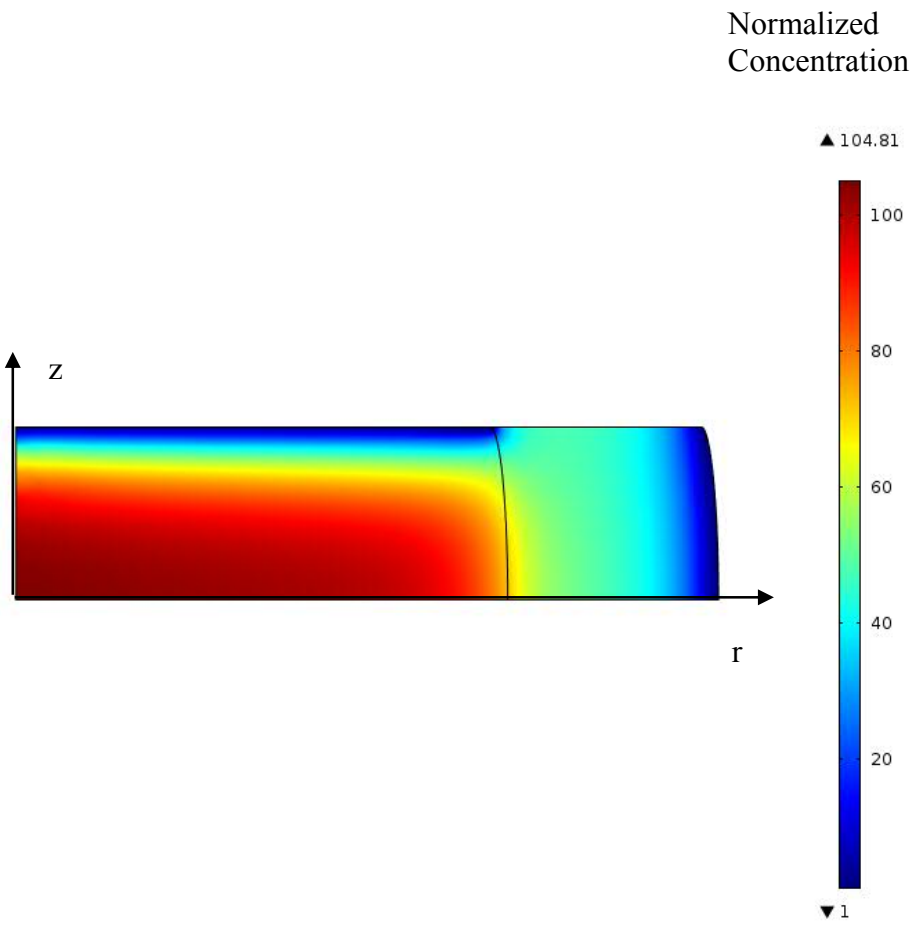

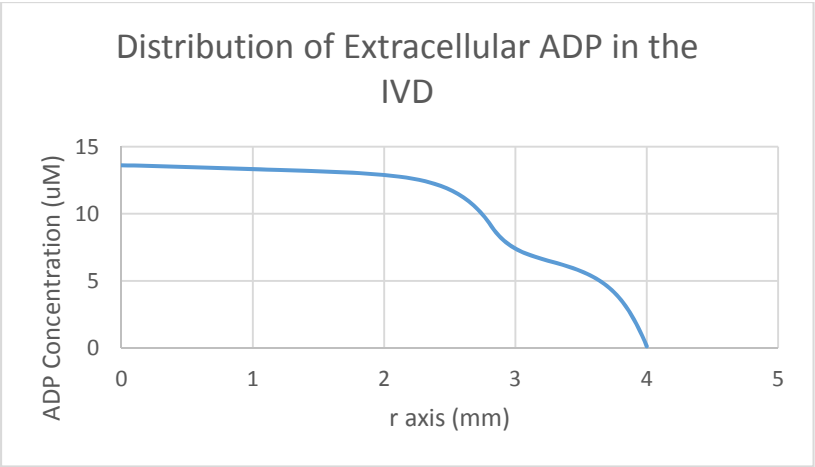

Figure 4-10: ADP concentration after dynamic compression. Dynamic compression was at frequency 0.05 Hz for t= 2 hr. The maximum ADP concentration was 13.6 µM. Boundary conditions were an initial strain of 10% for static compression and 5% strain with sinusoidal displacement for dynamic compression.

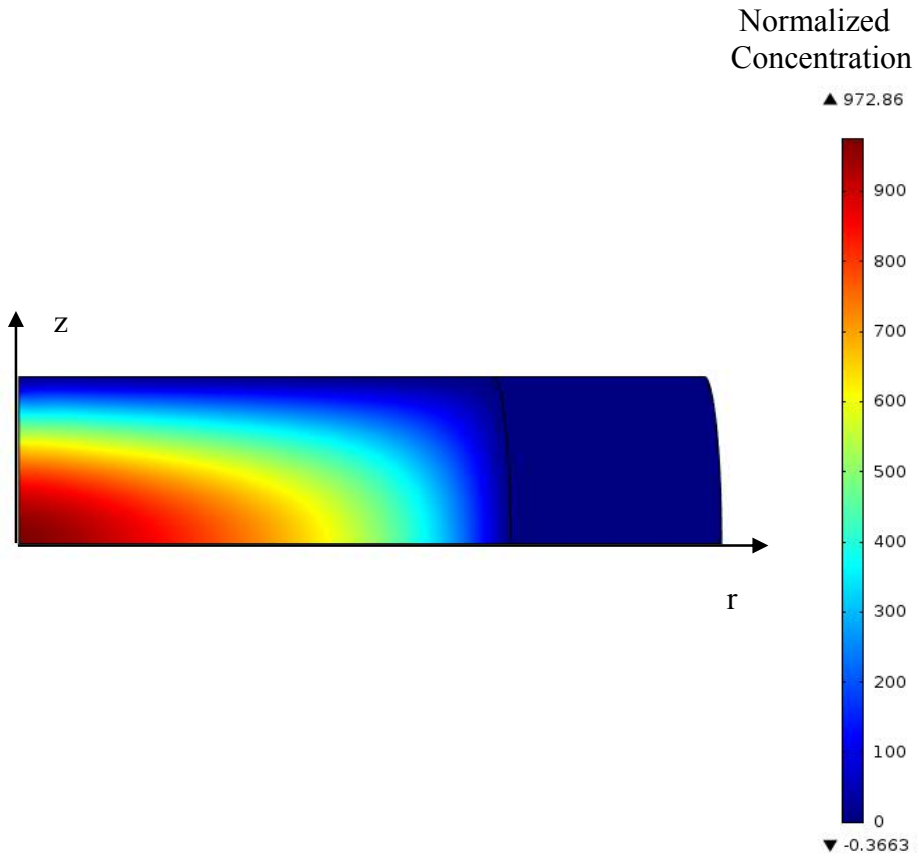

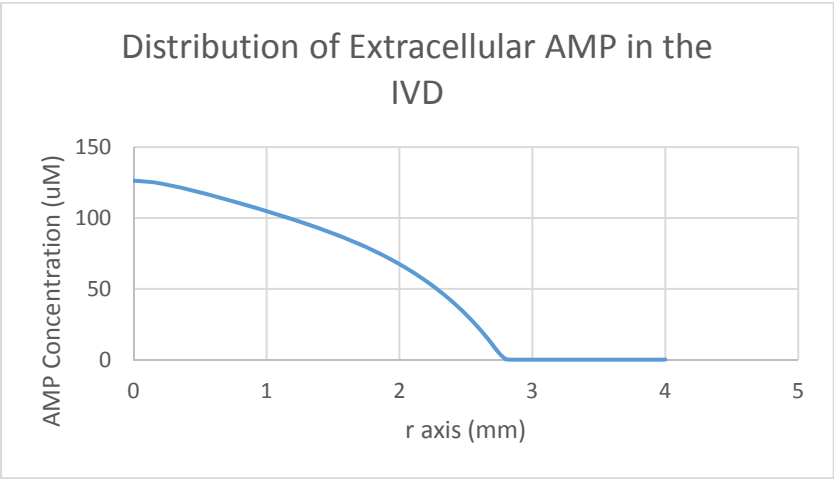

Figure 4-11: AMP concentration after dynamic compression. Dynamic compression was at frequency 0.05 Hz for t= 2 hr. The maximum AMP concentration was 126.5 µM. Boundary conditions were an initial strain of 10% for static compression and 5% strain with sinusoidal displacement for dynamic compression.

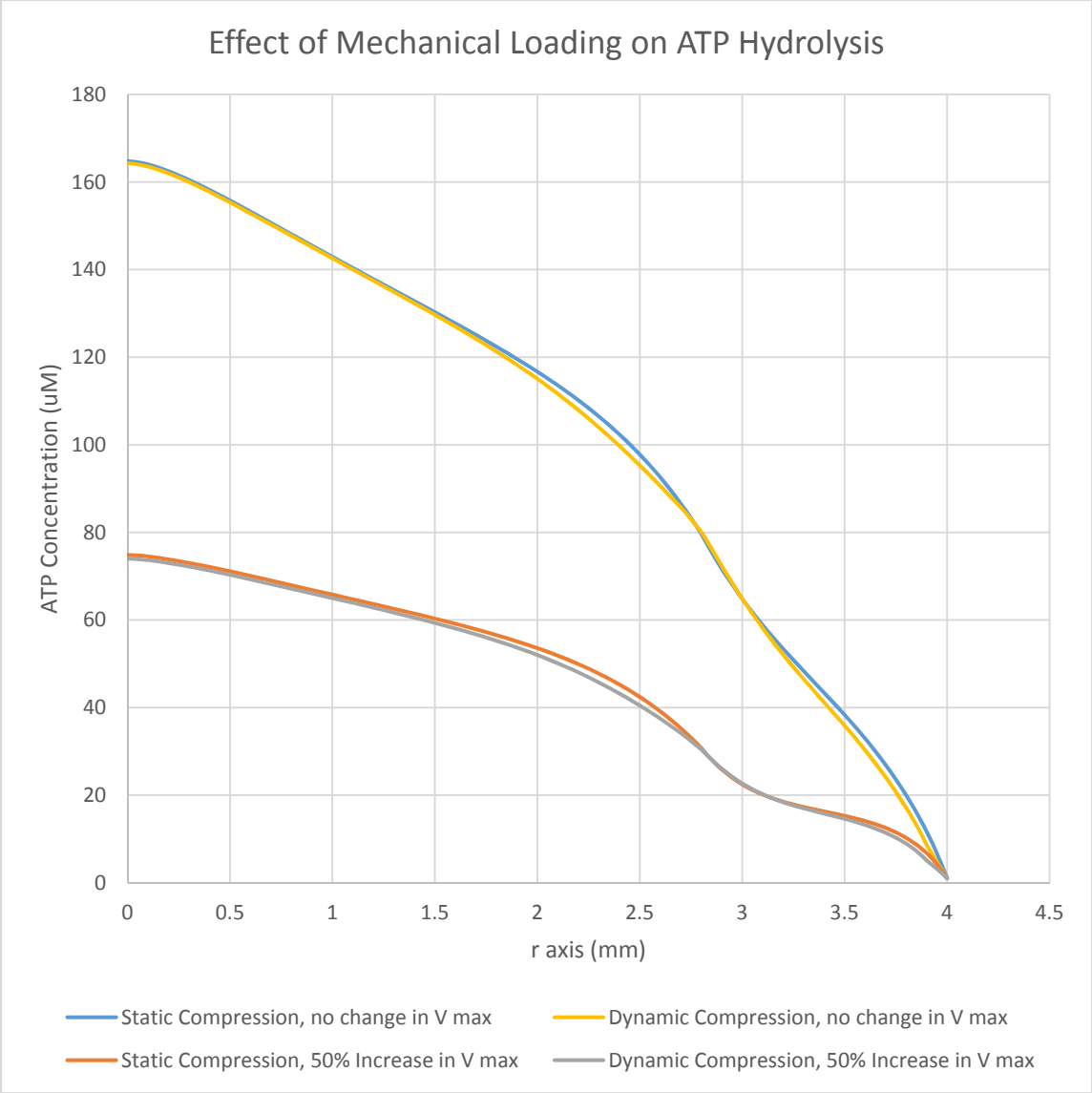

Figure 4-12: Effect of 50% increase in V_1 on extracellular ATP concentration. When V_1 was increased by 50% under dynamic compression, the maximum extracellular ATP concentration decreased by 35.7% from 165 µM to 74 µM with static compression. Without a change in V_1, dynamic compression decreased the ATP concentration by 1.0%.

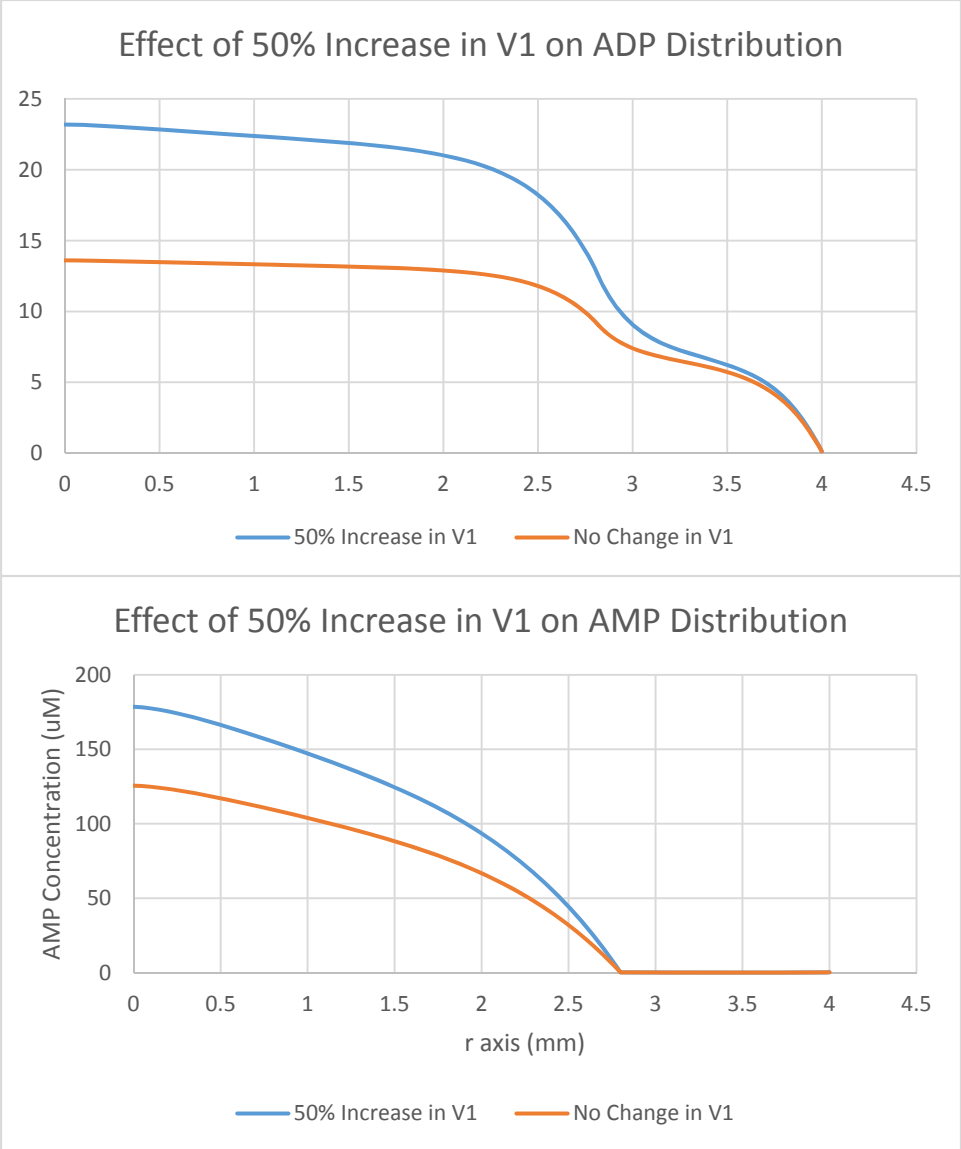

Figure 4-13: Effect of 50% increase in V_1 on ADP and AMP distribution. The ADP concentration increased 70.5% from 13.6 µM to 23.2 µM after a 50% increase in V_1. The AMP concentration increased 42.2% from 125.5 to 178.5 µM.

Chapter 5—Discussion

5.1 Summary

This study presents the first known finite element model to analyze the distribution of extracellular ATP concentration and its adenine derivatives in the IVD. The theoretical analysis, which is based on multiphasic mechano-electrochemical theory for charged hydrated soft tissues, predicts the extracellular ATP distribution described by Wang et al. (2013) and the effect of mechanical loading on the IVD. The concentration of ATP and its adenine derivatives may be altered under mechanical compression and promote ATP hydrolysis. In addition, experiments to measure extracellular ATP hydrolysis indicated a significant difference in Michaelis-Menten parameters between NP and AF cells.

5.2 Mechanical Loading of IVD Cells

After static compression was applied, dynamic compression at f = 0.05 Hz led to a decrease in ATP and adenine derivative concentration. It is consistent with our previous study that showed dynamic loading promoted solute transport (56). Assuming that V_1 remained constant, mechanical loading induced a small decrease in ATP concentration (1.0%). Once V_1 was increased by 50% to model an intrinsic effect on IVD cells, results were comparable to the finding by Wang et al. (2013) showing an approximately 50% decrease in the extracellular ATP concentration in the IVD under dynamic loading. As a result, the model shows that mechanical loading may promote hydrolysis of ATP. Since ATP is hydrolyzed by ecto-nucleotidases, mechanical loading may promote enzymatic breakdown of ATP or upregulate enzyme production of IVD cells. Previous studies have shown that changes in cellular and enzymatic activity occur in IVDs after mechanical

compression (57). Moreover, dynamic compression has been shown to increase the ATP concentration in both the AF and NP region of the IVD (9).

In addition, a significant increase in ADP and AMP after mechanical compression was expected because the conservation of mass would predict an inverse relationship between ATP hydrolysis and ADP production. According to mass conservation, the degradation of ATP is expected to lead to the generation of ADP. This result was observed in the model after mechanical compression, as the ADP and AMP concentration increased when the ATP concentration decreased. Thus, the theoretical model can predict the general change in adenine nucleotide concentration.

Long-term compressive loading is known to decrease the disc height and decrease fluid content that reduces solute transport (58). IVD cells use nutrients to generate concentration gradients whose magnitude depend on the balance between transport rate and cellular activity (7). Reduced solute diffusivity may alter the local solute concentration, inducing a change in metabolic rate of neutral solutes that acts to restore equilibrium levels (56). At the equilibrium state, the balance between the metabolism and transport of solute determines local solute concentration. This example of extracellular ATP homeostasis has been reported to involve the balance of ectoenzyme activity in animals (59).

Dynamic mechanical loading may also induce solute transport by enhancing convection. While diffusion is the predominant mode of transport in avascular tissue such as the IVD, convective transport is only a minor factor. Since ATP is a relatively small solute, with a molecular mass of 507.81 g/mol, fluid flow induced by mechanical loading is not known to enhance the transport of low-weight solutes (60). Therefore, dynamic

compression only induces small changes in ATP distribution in the IVD with a minimal intrinsic effect on IVD cells.

The exact mechanism of mechanical loading inducing ATP hydrolysis has not been fully elucidated in the literature. The mechanism might be mediated by a mechanotransduction pathway (61). Mechanotransduction is reported to contain three coupled processes: mechanosensing, signaling pathway, and effector-cell response (62). This coupling has been studied in chondrocytes and is assumed to be similar in IVD cells. In chondrocytes, mechanical loading opens connexin hemichannels to allow the release of ATP, which may then activate P2 receptors to trigger downstream signaling cascades to alter cell function. A similar mechanotransduction pathway might also exist in the IVD. The mechanism for this pathway could involve an alteration in local fixed charge density (c^F) and nutrient transport due to reduced fluid content (63). However, the sequence from mechanical signal to biochemical response needs to be further investigated.

5.3 ATP Hydrolysis Experiment

Based on the results of the experiment, NP and AF cells in the IVD may differ in extracellular ATP hydrolysis rate. Since the cell density in the AF region is higher than the NP region (9000 cells/mm³ and 4000 cells/ mm³ for human AF and NP, respectively), the extracellular ATP hydrolysis rate may be significantly higher for the AF region. In addition, the V_1 for AF cells may be significantly higher than NP cells.

Some difficulties with the ATP hydrolysis experiment included optimization of experimental design and conditions. Determination of the optimal ATP concentration involved several retests of the experiment because a significant difference in injected ATP concentration was found between each IVD cell type. The optimal ATP concentration

could depend on experimental conditions such as volume of media and time period. In addition, some variability in ATP hydrolysis was observed between samples. Possible sources of variability included isolation of IVD cells from different pigs and the size of agarose gel pieces in the chamber.

Michaelis-Menten parameters derived from the chondrocyte data by Hatori et al. (1995) was comparable to data from AF cells. On average, the V_1 calculated from AF cells was 1.8% greater than that from chondrocyte data (55). However, the K_M was 89.2% lower than that calculated from chondrocyte data (14.14 μM versus 131.04 μM). A smaller K_M means higher affinity for its substrate, so specific enzymes in porcine cells may catalyze ATP hydrolysis reactions with greater kinetic efficiency. The V_1 value for AF cells is about 53.9% greater than the concentration for NP cells. Thus, AF cells may exhibit a greater extracellular ATP hydrolysis rate than NP cells because of a higher reaction velocity.

The extracellular ATP hydrolysis rate may be significantly greater for AF cells compared to NP cells. NP cells are physiologically and structurally distinct from AF cells with different embryonic origins and a higher amount of proteoglycan (64, 65). Differences between these two cell types *in vivo* could be maintained during *in vitro* experiments. These differences might explain why the ATP hydrolysis rate in NP cells differs significantly from AF cells. Moreover, a high correlation coefficient between the experimental data and theoretical curve fitting suggest that V_1 and K_1 were accurately determined.

A previous study reported that notochordal NP cells may be more metabolically active than AF cells because ATP production is higher in notochordal NP cells (1). However, this study suggests that the extracellular ATP hydrolysis rate for AF cells may be significantly greater than that of NP cells. This difference shows that intracellular ATP

consumption may not be comparable to extracellular ATP hydrolysis. In addition, the NP cell type is different from the study by Salvatierra et al. (2011), since according to Guehring et al. (2010), mature chondrocytic-like NP cells are assumed to be predominant in the adult IVD and may contain different mechanical properties from notochordal NP cells (1, 66). Chondrocyte-like NP cells are the primary mature cell type in the IVD, which differs from notochordal-like NP cells in proteoglycan synthesis (4). According to Smith et al. (2011), compressive loading decreased the number of notochordal-like cells and increased the number of mature NP cells, especially as the nutrient and oxygen levels decreased in avascular tissue (67).

One inherent limitation of this study is the lack of Michaelis-Menten parameter values for adenine derivatives in the IVD, ADP and AMP. Theoretical curve fitting of chondrocyte data from Hatori et al. (1995) are estimates for these values (55). However, this theoretical model may predict these unknown values when *in vivo* measurements are difficult to measure. A high accumulation of ADP and AMP in the IVD could be significant, since ADP may trigger cellular activities by purinergic P2Y receptors (13). AMP can be hydrolyzed into adenosine, which can function in cellular adenosine uptake (68). In order to predict the distribution of adenine derivatives more accurately, more detailed information about the hydrolysis rate of these solutes is needed.

Chapter 6—Conclusion

6.1 Summary

This thesis is the first to study the distribution of extracellular ATP using multiphasic mechano-electrochemical theory in a finite element model. Mechanical loading may alter the concentration of ATP and its adenine derivatives. Moreover, the ATP concentration may decrease because ATP hydrolysis is promoted. After an increase in the value of V_1, ADP and AMP concentrations increase in response to mechanical loading. Experiments to measure ATP hydrolysis rate show that for AF cells, the V_1 is about 53.9% greater than the V_1 for NP cells. Experimental determination of V_1 and K_1 for ATP hydrolysis, once input into the theoretical model, show an ATP distribution in the general range described by Wang et al. (2013) (9). This study presents extracellular ATP accumulation and its adenine derivatives in the IVD using a finite element model.

6.2 Future Work

Binding reactions of ATP and its adenine derivatives to other molecules have not been considered in the model, which would reduce the amount of free ATP available and the rate of ATP diffusion in the IVD (44). This binding phenomena has not yet been characterized for ATP, but ATP may competitively bind with the ECM or other solutes. It is a limitation of the theoretical model that could be implemented in future studies. K_M and V_{max} of adenine derivatives (ADP, AMP) in the theoretical model may vary between AF and NP cells, since the two cell types differ in phenotypic expression (6). Incorporating variations in Michaelis-Menten parameters can improve the accuracy of the solute

distribution in different regions of the IVD. In addition, the identity of enzymes catalyzing ATP hydrolysis specifically in the IVD should be determined. It can be performed using enzyme assays, which plot reaction velocity V with substrate concentration [S], which can verify experimental data. It would improve the accuracy of Michaelis-Menten parameters used in the theoretical model. In addition, Michaelis-Menten parameters for adenosine have not yet been determined, which would help researchers study adenosine distribution and uptake in the IVD (69).

In the future, the finite element model can integrate aspects of disc degeneration by simulating changes in CEP permeability and solute transport. The boundary above the NP region can be restricted to 50% permeable in a simulation of endplate calcification. As the disc degenerates, a loss of hydration and disc integrity in the fibrocartilage occurs (70). In addition to reducing the nutrient supply, the effect of reduced endplate permeability on extracellular ATP distribution could be investigated (5).

References

1. Salvatierra JC, Yuan TY, Fernando H, Castillo A, Gu WY, Cheung HS, et al. Difference in energy metabolism of annulus fibrosus and nucleus pulposus cells of the intervertebral disc. Cell Mol Bioeng. 2011;4(2):302-10.

2. Marchand F, Ahmed AM. Investigation of the laminate structure of lumbar disc anulus fibrosus. Spine (Phila Pa 1976). 1990;15(5):402-10.

3. Bae WC, Du J, Bydder GM, Chung CB. Conventional and ultrashort time-to-echo magnetic resonance imaging of articular cartilage, meniscus, and intervertebral disk. Top Magn Reson Imaging. 2010;21(5):275-89.

4. Smith LJ, Nerurkar NL, Choi KS, Harfe BDE, D.M. Degeneration and regeneration of the intervertebral disc: lessons from development. Dis Model Mech. 2011;4(1):31-41.

5. Jackson AR, Huang CY, Brown MD, Gu WY. 3D finite element analysis of nutrient distributions and cell viability in the intervertebral disc: effects of deformation and degeneration. J Biomech Eng. 2011;133(9):091006.

6. Huang CY, Yuan TY, Jackson AR, Hazbun L, Fraker C, Gu WY. Effects of low glucose concentrations on oxygen consumption rates of intervertebral disc cells. Spine (Phila Pa 1976). 2007;32(19):2063-9.

7. Mokhbi Soukane D, Shirazi-Adl A, Urban JP. Investigation of solute concentrations in a 3D model of intervertebral disc. European spine journal : official publication of the European Spine Society, the European Spinal Deformity Society, and the European Section of the Cervical Spine Research Society. 2009;18(2):254-62.

8. van der Werf M, Lezuo P, Maissen O, van Donkelaar C, Ito K. Inhibition of vertebral endplate perfusion results in decreased intervertebral disc intranuclear diffusive transport. J Anat. 2007;211(6):769-74.

9. Wang C, Gonzales S, Levene H, Gu W, Huang CY. Energy metabolism of intervertebral disc under mechanical loading. Journal of Orthopaedic Research. 2013;31(11):1733-8.

10. Regateiro FS, Cobbold SP, Waldmann H. CD73 and adenosine generation in the creation of regulatory microenvironments. Clin Exp Immunol. 2013;171(1):1-7.

11. Burnstock G. Pathophysiology and therapeutic potential of purinergic signaling. Pharmacol Rev. 2006;58(1):58-86.

12. Coppi E, Pugliese A, Urbani S, Melani A, Cerbai E, Mazzanti B, et al. ATP modulates cell proliferation and elicits two different electrophysiological responses in human mesenchymal stem cells. Stem Cells. 2007;25(7):1840-9.

13. Czajkowski R, Banachewicz W, Ilnytska O, Drobot L, Baranska J. Differential effects of P2Y1 and P2Y12 nucleotide receptors on ERK1/ERK2 and phosphatidylinositol 3-kinase signalling and cell proliferation in serum-deprived and nonstarved glioma C6 cells. Br J Pharmacol 2004;141(3):497-507.

14. Niermann KJ, Olsen NJ, Park JH. Magnesium abnormalities of skeletal muscle in dermatomyositis and juvenile dermatomyositis. Arthritis Rheum. 2002;46(2):475-88.

15. Vinogradov AD. Steady-state and pre-steady-state kinetics of the mitochondrial F(1)F(o) ATPase: is ATP synthase a reversible molecular machine? J Exp Biol 2000;203(Pt 1):41-9.

16. Leal DB, Streher CA, Neu TN, Bittencourt FP, Leal CA, da Silva JE, et al. Characterization of NTPDase (NTPDase1; ecto-apyrase; ecto-diphosphohydrolase; CD39; EC 3.6.1.5) activity in human lymphocytes. Biochim Biophys Acta. 2005;1721(1-3):9-15.

17. Kukulski F, Lévesque SA, Lavoie EG, Lecka J, Bigonnesse F, Knowles AF, et al. Comparative hydrolysis of P2 receptor agonists by NTPDases 1, 2, 3 and 8. Purinergic Signal. 2005;1(2):193-204.

18. Graff RD, Lazarowski ER, Banes AJ, Lee GM. ATP release by mechanically loaded porcine chondrons in pellet culture. Arthritis Rheum. 2000;43(7):1571-9.

19. Erga K, Seubert C, Liang H, Wu L, Shryock J, Belardinelli L. Role of A2A-adenosine receptor activation for ATP-mediated coronary vasodilation in guinea-pig isolated heart. Br J Pharmacol 2000;130(5):1065-75.

20. Haskó G, Cronstein B. Regulation of inflammation by adenosine. Front Immunol. 2013;4(85).

21. Schinle F, Crider PE, Vonderach M, Weis P, Hampe O, Kappes MM. Spectroscopic and theoretical investigations of adenosine 5′-diphosphate and adenosine 5′-triphosphate dianions in the gas phase. Phys Chem Chem Phys. 2013;15(18):6640-50.

22. Zhang Y. Phenomenological analysis of ATP dependence of motor proteins. PloS one. 2012;7(3):e32717.

23. Van Aubel RA, Peters JG, Masereeuw R, Van Os CH, Russel FG. Multidrug resistance protein mrp2 mediates ATP-dependent transport of classic renal organic anion p-aminohippurate. American journal of physiology Renal physiology. 2000;279(4):F713-7.

24. Ohshima H, Urban JP, Bergel DH. Effect of static load on matrix synthesis rates in the intervertebral disc
measured in vitro by a new perfusion technique. J Orthop Res 1995;13(1):22-9.

25. Walsh AJ, Lotz JC. Biological response of the intervertebral disc to dynamic loading. J Biomech. 2004;37(3):329-37.

26. Maclean JJ, Lee CR, Alini M, Iatridis JC. Anabolic and catabolic mRNA levels of the intervertebral disc vary with the magnitude and frequency of in vivo dynamic compression. J Orthop Res. 2004;22(6):1193-200.

27. Setton LA, Chen J. Mechanobiology of the intervertebral disc and relevance to disc degeneration. J Bone Joint Surg Am 2006;88 Suppl(2):52-7.

28. Fernando H, Czamanski J, Yuan T, Gu W, Salahadin A, Huang CY. Mechanical loading affects the energy metabolism of intervertebral disc cells. J Orthop Res. 2011;29(11):1634-41.

29. Millward-Sadler SJ, Wright MO, Flatman PW, Salter DM. ATP in the mechanotransduction pathway of normal human chondrocytes. Biorheology. 2004;41(3-4):567-75.

30. Chowdhury T, Knight M. Purinergic pathway suppresses the release of .NO and stimulates proteoglycan synthesis in chondrocyte/agarose constructs subjected to dynamic compression. J Cell Physiol 2006;209(3):845-53.

31. Goldsmith A, Hayes A, Clift S. Application of finite elements to the stress analysis of articular cartilage. Med Eng Phys. 1996;18(2):89-98.

32. Hollingsworth NT, Wagner DR. Modeling shear behavior of the annulus fibrosus. J Mech Behav Biomed Mater. 2011;4(7):1103-14.

33. Oomens CWJ, De Heus HJ, Huyghe JM, Nelissen L, Janssen JD. Validation of the triphasic mixture theory for a mimic of intervertebral disk tissue. Biomimetics. 1995;3(4).

34. Huyghe JM. Quadriphasic mechanics of swelling incompressible porous media. International Journal of Engineering Science. 1997;35(8):793-802.

35. Mow VC, Kuei SC, Lai WM, Armstrong CG. Biphasic creep and stress relaxation of articular cartilage in compression? Theory and experiments. Journal of biomechanical engineering. 1980;102(1):73-84.

36. Lai WM, Hou JS, Mow VC. A triphasic theory for the swelling and deformation behaviors of articular cartilage. Journal of biomechanical engineering. 1991;113(245-58).

37. Nguyen VX, Abousleiman YN. Incorporating electrokinetic effects in the porochemoelastic inclined wellbore formulation and solution. An Acad Bras Cienc. 2010;82(1):195-222.

38. Gu WY, Lai WM, Mow VC. Effects of hydration and fixed charge density on fluid transport in charged hydrated soft tissue. Journal of biomechanical engineering. 1998;120(169-80).

39. Gu WY, Justiz MA, Yao H. Electrical conductivity of lumbar anulus fibrosis: effects of porosity and fixed charge density. Spine (Phila Pa 1976). 2002;27(21):2390-5.

40. Gu WY, Yao H, Huang CY, Cheung HS. New insight into deformation-dependent hydraulic permeability of gels and cartilage, and dynamic behavior of agarose gels in confined compression. J Biomech. 2003;36(4):593-8.

41. Yao H, Gu WY. Convection and diffusion in charged hydrated soft tissues: a mixture theory approach. Biomech Model Mechanobiol. 2007;6(1-2):63-72.

42. Yao H, Gu WY. Physical signals and solute transport in cartilage under dynamic unconfined compression: finite element analysis. Ann Biomed Eng. 2004;32(3):380-90.

43. Zhu Q, Jackson AR, Gu WY. Cell viability in intervertebral disc under various nutritional and dynamic loading conditions: 3d finite element analysis. J Biomech. 2012;45(16):2769-77.

44. Huang CY, Travascio F, Gu WY. Quantitative analysis of exogenous IGF-1 administration of intervertebral disc through intradiscal injection. J Biomech. 2012;45(7):1149-55.

45. Sun DN, Gu WY, Guo XE, Lai WM, Mow VC. A mixed finite element formulation of triphasic mechano-electrochemical theory for charged, hydrated biological soft tissues. International Journal for Numerical Methods in Engineering. 1999;45(10):1375–402.

46. Hussain M, Natarajan RN, G C, An HS, Andersson GB. Relative contributions of strain-dependent permeability and fixed charged density of proteoglycans in predicting cervical disc biomechanics: a poroelastic C5-C6 finite element model study. Med Eng Phys. 2011;33(4):438-045.

47. Gu WY, Yao H. Effects of hydration and fixed charge density on fluid transport in charged hydrated soft tissues. Ann Biomed Eng. 2003;31(10):1162-70.

48. Gu WY, Yao H, Vega AL, Flagler D. Diffusivity of ions in agarose gels and intervertebral disc: effect of porosity. Annals of biomedical engineering. 2004;32(12):1710-7.

49. Zhang Y, Markova D, Im HJ, Hu W, Thonar EJ, He TC, et al. Primary bovine intervertebral disc cells transduced with adenovirus overexpressing 12 BMPs and Sox9 maintain appropriate phenotype. Am J Phys Med Rehabil. 2009;88(6):455-63.

50. Marques SM, Esteves da Silva JC. Firefly bioluminescence: a mechanistic approach of luciferase catalyzed reactions. IUBMB Life. 2009;61(1):6-17.

51. Furuya K, Sokabe M, Grygorczyk R. Real-time luminescence imaging of cellular ATP release. Methods. 2013;S1046-2023(13):00305-8.

52. Michel AD, Xing M, Humphrey PPA. Serum constituents can affect 2′-& 3′-O-(4-benzoylbenzoyl)-ATP potency at P2X7 receptors. Br J Pharmacol. 2001;132(7):1501-8.

53. Gorman M, Feigl E, Buffington CW. Human plasma ATP concentration. Clin Chem 2007;53(2):318-25.

54. Jabs C, Ferrell W, Robb H. Plasma ADP levels: direct determination with luciferase luminescence using a biometer. Clin Biochem. 1978;11(5):190-3.

55. Hatori M TC, Debolt K, Pacifici M, Shapiro IM. Adenine nucleotide metabolism by chondrocytes in vitro: role of ATP in chondrocyte maturation and matrix mineralization. J Cell Physiol 1995 165(3):468-74.

56. Huang CY, Gu WY. Effects of mechanical compression on metabolism and distribution of oxygen and lactate in intervertebral disc. J Biomech. 2008;41(6):1184-96.

57. Walter BA, Korecki CL, Purmessur D, Roughley PJ, Michalek AJ, Iatridis JC. Complex loading affects intervertebral disc mechanics and biology. Osteoarthritis Cartilage. 2011;19(8):1011-8.

58. Schmidt H, Galbusera F, Rohlmann A, Shirazi-Adl A. What have we learned from finite element model studies of lumbar intervertebral discs in the past four decades? J Biomech. 2013;46(14):2342-55.

59. Chivasa S, Ndimba BK, Simon WJ, Lindsey K, Slabas AR. Extracellular ATP functions as an endogenous external metabolite regulating plant cell viability. Plant Cell 2005;17(11):3019-34.

60. Ferguson S, Ito K, Nolte L. Fluid flow and convective transport of solutes within the intervertebral disc. J Biomech. 2004;37(2):213-21.

61. Garcia M, Knight M. Cyclic loading opens hemichannels to release ATP as part of a chondrocyte mechanotransduction pathway. J Orthop Res. 2010;28(4):510-5.

62. Neidlinger-Wilke C GF, Pratsinis H, Mavrogonatou E, Mietsch A, Kletsas D, Wilke HJ. Mechanical loading of the intervertebral disc: from the macroscopic to the cellular level. Eur Spine J. 2013.

63. Iatridis JC MJ, Roughley PJ, Alini M. Effects of mechanical loading on intervertebral disc metabolism in vivo. J Bone Joint Surg Am. 2006;88(2):41-6.

64. Vieira VP, Rocha JB, Stefanello FM, Balz D, Morsch VM, Schetinger MR. Heparin and chondroitin sulfate inhibit adenine nucleotide hydrolysis in liver and kidney membrane enriched fractions. The international journal of biochemistry & cell biology. 2001;33(12):1193-201.

65. Choi KS, Cohn MJ, Harfe BD. Identification of nucleus pulposus precursor cells and notochordal remnants in the mouse: implications for disk degeneration and chordoma formation. Developmental dynamics : an official publication of the American Association of Anatomists. 2008;237(12):3953-8.

66. Guehring T, Nerlich A, Kroeber M, Richter W, Omlor GW. Sensitivity of notochordal disc cells to mechanical loading: an experimental animal study. European spine journal : official publication of the European Spine Society, the European Spinal Deformity Society, and the European Section of the Cervical Spine Research Society. 2010;19(1):113-21.

67. Smith LJ, Nerurkar NL, Choi KS, Harfe BDE, D.M. Degeneration and regeneration of the intervertebral disc: lessons from development. Dis Model Mech 2011;4(1):31-41.

68. Riksen NP RG, Boers GH, Blom HJ, van den Broek PH, Smits P. Enhanced cellular adenosine uptake limits adenosine receptor stimulation in patients with hyperhomocysteinemia. Arterioscler Thromb Vasc Biol 2005;25(1):109-14.

69. Mistry D, Chambers MG, Mason RM. The role of adenosine in chondrocyte death in murine osteoarthritis and in a murine chondrocyte cell line. Osteoarthritis Cartilage. 2006;14(5):486-95.

70. Zirbel SA, Stolworthy DK, Howell LL, Bowden AE. Intervertebral disc degeneration alters lumbar spine segmental stiffness in all modes of loading under a compressive follower load. Spine J. 2013;13(9):1134-47.